TROLL 4.0: representing water and carbon fluxes, leaf phenology, and intraspecific trait variation in a mixed-species individual-based forest dynamics model – Part 2: Model evaluation for two Amazonian sites

Sylvain Schmitt[1,2,3], Fabian J. Fischer[4], James G. C. Ball[5], Nicolas Barbier[3], Marion Boisseaux[6], Damien Bonal[7], Benoit Burban[8], Xiuzhi Chen[9], Géraldine Derroire[1,2,10], Jeremy W. Lichstein[11], Daniela Nemetschek[4], Natalia Restrepo-Coupe[12], Scott Saleska[12], Giacomo Sellan[10], Philippe Verley[3], Grégoire Vincent[3], Camille Ziegler[6], Jérôme Chave[13], Isabelle Maréchaux[3]

[1]CIRAD, UPR Forêts et Sociétés, F-34398, Montpellier, France
[2]Forêts et Sociétés, Univ Montpellier, CIRAD, Montpellier, France
[3]AMAP, Univ Montpellier, INRAE, IRD, CIRAD, CNRS, F-34000 Montpellier, France
[4]School of Biological Sciences, University of Bristol, 24 Tyndall Avenue, Bristol, BS8 1TQ, UK
[5]Department of Plant Sciences, University of Cambridge, Downing Street, Cambridge, CB2 3EA, UK
[6]Univ. Bordeaux, INRAE, BIOGECO, 33612 Pessac, France
[7]Université de Lorraine, AgroParisTech, INRAE, UMR Silva, 54000 Nancy, France
[8]INRAE, UMR EcoFoG (Agroparistech, Cirad, CNRS, Université des Antilles, Université de la Guyane), Campus Agronomique, 97310 Kourou, French Guiana
[9]School of Atmospheric Sciences, Sun Yat-sen University, Guangzhou 510275, China
[10]Cirad, UMR EcoFoG (Agroparistech, CNRS, INRAE, Université des Antilles, Université de la Guyane), Campus Agronomique, 97310 Kourou, French Guiana
[11]Department of Biology, University of Florida, Gainesville, Florida 32611, USA
[12]University of Arizona, Ecology & Evolutionary Biology, Tucson, Arizona, United States of America
[13]Centre de Recherche Biodiversité et Environnement, UMR5300, CNRS, Université Paul Sabatier, IRD, INPT, Toulouse Cedex 9, France

Correspondence to: Sylvain Schmitt (sylvain.schmitt@cirad.fr)

26   **Summary.** We evaluate the capability of TROLL 4.0, a simulator of forest dynamics, to represent tropical forest structure,
27   diversity and functioning in two Amazonian forests. Evaluation data include forest inventories, carbon and water fluxes
28   between the forest and the atmosphere, and leaf area and canopy height from remote-sensing products. The model realistically
29   predicts the structure and composition, and the seasonality of carbon and water fluxes at both sites.
30
31
32
33   **Abstract.** TROLL 4.0 is an individual-based forest dynamics model that jointly simulates the structure, diversity and
34   functioning of tropical forests, including their water balance, carbon fluxes and leaf phenology, while accounting for
35   intraspecific trait variation for a large number of species. In a companion paper, we describe how the model represents the
36   physiological and demographic processes that control the tree life cycle in a one-metre-resolution spatially-explicit scene and
37   uses plant functional traits measurable in the field to parameterize such processes across species and individuals (Maréchaux
38   et al., submitted companion paper). Here we evaluate the performance of TROLL 4.0 for two Amazonian sites with contrasting
39   soil and climate properties. We assessed the model's ability to represent forest structure and composition using lidar-derived
40   canopy height distributions and forest inventories combined with information on plant functional traits. We also evaluated the
41   model's ability to represent carbon and water fluxes, as well as leaf area variation, at daily and fortnightly resolution over a
42   decade, using detailed information from on-site eddy covariance towers, satellite data and ground-based or air-borne lidar data.
43   We finally compared the responses of carbon and water fluxes to environmental drivers between simulated and observed data.
44   Overall, TROLL 4.0 provided a realistic representation of forests at both sites. The simulated canopy height distribution
45   showed a high correlation coefficient (CC) with observed aerial and satellite data (CC>0.92), while the species and functional
46   composition were well represented (CC>0.75). TROLL 4.0 also realistically simulated the seasonal variability of carbon and
47   water fluxes (CC>0.46) and their responses to environmental drivers, while capturing temporal variations in leaf area
48   (CC>0.76) and its partitioning in leaf age cohorts. However, TROLL 4.0 overestimated annual gross primary productivity at
49   both sites (mean RMSEP=0.94 kgC m^{-2} yr^{-1}) and evapotranspiration at one site (mean RMSEP=0.75 mm day^{-1}), likely due to
50   an underestimation of the soil water depletion and stomatal control during the dry season. This evaluation highlights the
51   potential of TROLL 4.0 to represent ecosystem fluxes and the structure and diversity of plant communities at a fine resolution,
52   paving the way for model predictions of the effects of climate change, fragmentation and forest management on forest structure
53   and dynamics.

1 Introduction

Tropical forests cover just 7% of the Earth's land surface, yet they play a disproportionately large role in the biosphere, store around 25% of terrestrial carbon and contribute to more than a third of global terrestrial productivity (Bonan 2008). Regionally, tropical forests recycle around a third of precipitation through evapotranspiration, contributing to the generation and maintenance of a humid climate (Harper et al., 2013), effects that extend well beyond the tropics (Lawrence & Vandecar 2015). However, tropical forests remain a major source of uncertainty in simulations of global biogeochemical cycles (Fisher et al., 2014; Koch et al., 2020).

As an illustration, for light-limited tropical forests, dynamic global vegetation models (DGVMs, Prentice et al., 2007) typically simulate a decrease in productivity with a seasonal decline in precipitation (Restrepo-Coupe et al., 2017, Chen et al., 2020), while observations from eddy covariance data point to an increase in gross primary productivity during the dry season (Guan et al., 2015; Aguilos et al., 2018). Similarly, simulated forest responses to experimental and natural droughts have highlighted large model-data discrepancies and variation across models (Powell et al., 2013; Joetzjer et al., 2014; Yao et al., 2023; Paschalis et al., 2022). Improving the representation of tropical forest functioning in models is needed to enhance our understanding and ability to predict biogeochemical cycles.

One challenge is to better integrate the structure, diversity and functioning of forests into vegetation models (Purves and Pacala, 2008; McMahon et al., 2011; Evans, 2012; Mokany et al., 2016). In spite of progress (Fisher et al., 2018), most models still adopt a coarse grained representation of vegetation, which makes it difficult to use field data to parameterize and evaluate the models. Also, several processes driving the variation of tropical forest productivity and water fluxes remain incompletely represented in vegetation models. These include water uptake by the root system and seasonal variation of leaf quantity and quality at the ecosystem-level, which are driven by leaf phenology and allocation processes at the individual-level (Chen et al., 2020; Wu et al., 2021; Restrepo-Coupe et al., 2017, Cusak et al., 2024).

In a companion paper, we described the individual-based forest dynamics model TROLL 4.0 (Maréchaux et al., submitted companion paper). This model jointly simulates tropical forest structure, diversity and functioning, including forest water balance, carbon fluxes and leaf phenology, and accounts for intraspecific trait variation for a large number of species. TROLL 4.0 represents the processes underlying ecosystem fluxes, such as leaf gas exchanges and their responses to environmental variation, and is thus similar to DVGMs in that respect, with its outputs comparable with data from eddy covariance towers. However, unlike DGVMs that are designed for global applications and typically represent plant diversity with a few functional types, TROLL 4.0 represents diversity at the species level (e.g., 10s to 100s of tropical tree species). TROLL 4.0 is spatially-explicit and represents plant community structure and diversity at a spatial resolution of one metre, which is consistent with that used by field ecologists. Physiological and demographic processes are integrated using a parameterisation based on plant traits measurable in the field, relying on recent knowledge in plant physiology and functional ecology. The individual-based,

88 species-specific and spatially explicit representation of forest structure and composition enables TROLL 4.0 outputs to be

89 directly compared with spatially explicit forest inventories, trait distributions or fine-scale remote sensing products.

90

91 In this paper, we evaluate TROLL 4.0 for two Amazonian sites with contrasting soil and climate properties. We parameterized

92 the model using functional trait and soil data at both sites. We first calibrated three major forest structure parameters using

93 inventory data, and then the three parameters of the phenological module that control leaf shedding as a function of soil water

94 availability using litterfall data. We then ran simulations and evaluated the model's representation of forest structure and

95 composition against independent data, including lidar-derived canopy height distribution, understory inventories and

96 functional trait distribution. We also assessed the model ability to represent carbon and water fluxes at daily resolution, as well

97 as leaf area variation at fortnightly resolution, against eddy covariance, satellite and terrestrial or drone lidar data. We finally

98 compared the response of simulated and observed fluxes to incoming radiation, vapour pressure deficit, temperature, and wind

99 speed. Finally, we discuss the potential model-data discrepancies and identify priorities for future developments.

2 Methods

101 TROLL represents individual trees explicitly in an aboveground voxelized space (1 m^3), in which light diffusion is modelled,

102 and in a belowground space, which consists of several layers with user-defined thickness and horizontal resolution (here 25

103 m^2). Belowground water flow is simulated using a bucket model. Each tree belongs to a species, and we provide as input

104 species-specific mean plant trait values and intraspecific trait variances and covariances. At recruitment, individual trait values

105 are randomly drawn from the intraspecific trait distribution. These traits parameterize the physiological and demographic

106 processes that govern the life cycle of trees, from recruitment to growth, seed dispersal, and finally death. Carbon assimilation

107 by trees is computed using the photosynthesis model of Farquhar, von Caemmerer and Berry (1980), coupled to the stomatal

108 conductance model of Medlyn et al. (2011), as a function of leaf micro-environmental conditions, tree access to water, and

109 leaf photosynthetic capacity and leaf respiration rate. Sugars produced during photosynthesis are used for tree respiration and

110 allocation to plant tissues, including foliar production, carbon storage and woody growth.

111

112 We conducted model calibration and evaluation at two lowland Amazon forest sites: the Paracou research station in French

113 Guiana (5°28'N, 52°92'W), hereafter Paracou (Gourlet-Fleury et al., 2004; Bonal et al., 2008), and the Tapajos National Forest

114 in Brazil in the K67 site also named BR-Sa1 (2°86'S, 54°96'W), hereafter Tapajos (Silver et al., 2000; Saleska et al., 2003).

115 Both sites are covered by a high biomass and species rich lowland moist tropical forest, and they present contrasting soil

116 characteristics and climate (Table 1). The two sites have been intensively monitored for several decades, mainly through

117 repeated forest inventories and eddy flux tower measurements.

118

119 At each site, we calibrated six global parameters, three parameters related to forest structure, to which TROLL is known to be

120 sensitive: the reference background mortality rate m, and the intercept a_{CR} and slope b_{CR} of the crown radius scaling relationship

121 (Table A1; Maréchaux and Chave, 2017; Fischer et al., 2019), and three parameters pertaining to the phenological module,

122 new to TROLL 4.0 ($a_{T,o}$, $b_{T,o}$ and δ_o; Table A1). In TROLL 4.0, the shedding of old leaves is accelerated as soil water

123 availability decreases (Maréchaux et al., submitted companion paper). When the leaf predawn water potential (ψ_{pd}, MPa) falls

124 below a threshold $\psi_{T,o}$ (MPa), the residence time of old leaves is decreased using a multiplicative factor $f_0 < 1$. The parameter

125 $\psi_{T,o}$ varies with the tree leaf drought tolerance and its size as follows:

$$\psi_{T,o} = min(a_{T,o} \times \pi_{tlp}, -0.01 \times h - b_{T,o})$$

126

127 where π_{tlp} is the leaf water potential at turgor loss point in MPa and h is the tree height in m. f_0 is decremented (resp.

128 incremented) by δ_o when $\psi_{pd} < \psi_{T,o}$ (resp. $\psi_{pd} > \psi_{T,o}$). The parameters $a_{T,o}$, $b_{T,o}$ and δ_o control the intensity and the

129 timing of the peak of litterfall under drying soil conditions. This scheme is consistent with field observations (Maréchaux et

130 al. submitted companion paper), uncertainties remain on the values of $a_{T,o}$, $b_{T,o}$ and δ_o however, and they need to be calibrated.

131 After calibration, we compared model outputs with site-specific data for evaluation at each site.

132

133 **Table 1: Site overview with climate, vegetation and soil properties.**

Variables	Units	Paracou	Tapajos	References
Climate				
Annual rainfall	mm	3,041	2,075	P: Aguilos et al., 2018; T: Silver et al., 2000
Average air temperature	°C	25.7	26.1	
Vegetation				
Aboveground biomass ($DBH \geq 10$)	Mg ha⁻¹	419	287	P: Rutishauser et al., 2010; T: Rice et al., 2004
Abundance ($DBH \geq 10$)	ha⁻¹	612	470	P: Derroire et al., 2023; T: Rice et al., 2004
Basal area ($DBH \geq 10$)	m² ha⁻¹	31	24	P: Derroire et al., 2023; T: Goncalves et al., 2018
Soil				
Type	-	Sandy clay loam	Clay	-
Depth	m	2.50	16.10	P: Hiltner et al., 2021; T: Nepstad et al.,

			2002	
Layer thickness (top to bottom)	m	0.10 / 0.23 / 0.40 / 0.80 / 0.97	0.10 / 0.40 / 1.00 / 2.50 / 12.10	-
Sand	%	65.25	37.27	P: Van Langenhove et al., 2021; T: Silver et al., 2000
Clay	%	21.50	60.09	
Silt	%	13.25	2.64	
Soil Organic Content	%	2.37	2.54	P: Van Langenhove et al., 2021; T:Quesada et al., 2010
Dry Bulk Density	g cm^{-3}	1.040	1.125	P: Van Langenhove et al., 2021; T: Silver et al., 2000
Cation Exchange Capacity	mEq 100g^{-1}	2.98	2.97	P: Sabatier et al., 1997; T:Quesada et al., 2010
pH		4.34	3.84	P: Sabatier et al., 1997; T:Quesada et al., 2010

2.1 Simulation inputs and climatic drivers

TROLL 4.0 uses 35 global parameters defined by the user and provided as inputs. These parameters relate to atmospheric constants, light transmission, leaf carbon acquisition, leaf shedding, tree carbon allocation, tree shape, reproduction, and death, and intraspecific trait variability (Table A1). Except for the three parameters of forest structure mentioned above and the three parameters of the leaf shedding module that have been calibrated at each site, all values are assumed site independent.

TROLL 4.0 requires trait parameters for each species: values need to be provided as input for six functional traits and three scaling parameters. The scaling parameters are species maximum diameter at breast height (dbh_{max}, cm), and parameters defining the relationship between height and diameter at breast height (dbh), which are the asymptotic height (h_{lim}, m) and the parameter a_h (see Maréchaux et al. submitted companion paper, Eqs (16) and (62)). We used forest inventories from Paracou (Derroire et al., 2023) and Tapajos (Goncalves et al., 2018) to create a species list for each site, and computed dbh_{max} as the 95th quantile of species diameter at breast height for species including more than 10 individuals. We used the TALLO global database of height and diameter measurements (Jucker et al., 2022) to infer species-specific values of h_{lim} and a_h for the 496 species of the database that are present in Amazonia (latitude between 10°N and 18°S and longitude between 39°W and 78°W;

148 n = 24,609 trees with a mean of 49.62 ±730 trees per species). Parameters a_h and h_{lim} were inferred using Bayesian inference

149 as follows:

150 $$log(h) \sim N[log(h_{lim} \times \frac{dbh}{a_h + dbh}), \sigma^2] \mid h_{lim} \sim N(h_{lim,0}, \sigma^2_h), a_h \sim N(a_{h,0}, \sigma^2_a)$$

151 with the logarithm of height (h, in m) following a normal distribution centred on the log of a Michaelis-Menten model with

152 asymptotic height h_{lim}, height-dbh scaling parameter a_h, and variance σ^2. The two species-specific parameters h_{lim} and a_h

153 are random parameters following a normal distribution centred respectively on $h_{lim,0}$ and $a_{h,0}$ with variances σ^2_h and σ^2_a.

154

155 The functional traits used in the parameterization include leaf area (LA, in cm^2), leaf mass per area (LMA, g m^{-2}), leaf nitrogen

156 content per dry mass (N, mg g^{-1}), leaf phosphorus content per dry mass (P, mg g^{-1}), leaf water potential at turgor loss point

157 (π_{tlp}, MPa), and wood specific gravity (wsg, g cm^{-3}). We used several datasets to retrieve species-specific mean values for

158 these traits (Vleminckx et al. 2021, Boisseaux et al., submitted; Kattge, Bönisch, and al., 2020; Maréchaux et al., 2015;

159 Maréchaux et al., 2019; Nemetschek et al., 2024; Ziegler et al., 2019). Finally, we used predictive mean matching (Van Buuren

160 and Groothuis-Oudshoorn, 2011) to impute missing trait values for a_h, h_{lim}, dbh_{max}, and π_{tlp} only. Overall, this procedure

161 leads to a parameterization of 114 species for Paracou and 113 species for Tapajos. These species pools are representative of

162 the functional trait spaces of the two sites (Fig. A1).

163

164 TROLL 4.0 requests nine soil parameters to describe the texture, depth and chemistry. These were gathered from the literature,

165 assuming a single soil type and depth per site for simplicity and setting the number of soil layers to five (Table 1). Testing the

166 influence of horizontal and vertical soil heterogeneity on model outputs is left for future work.

167

168 TROLL 4.0 simulations are forced with six climatic drivers. Two of them are daily: cumulative rainfall (mm), and average

169 nighttime temperature (°C). The remaining four drivers are provided every half hour during the daytime (defined below):

170 incoming shortwave radiation (SW, W m^{-2}), temperature (T, °C), vapour pressure deficit (VPD, kPa), and wind speed (WS, m

171 s^{-1}). Historical time series for these climatic variables have been retrieved from the FLUXNET 2015 dataset (Pastorello et al.,

172 2020), which provides standardised data from eddy flux towers located at each site (2004-2014 for Paracou, and 2002-2011

173 for Tapajos). However, at Tapajos, rainfall data from FLUXNET 2015 is not reliable due to issues with rain gauges (Restrepo-

174 Coupe et al., 2017). Instead, we used rainfall data from the ERA5-Land reanalysis dataset (Muñoz-Sabater et al., 2021)

175 available at hourly resolution between 2002 and 2011. For other climatic variables, data from ERA5-Land showed high

176 correlation with FLUXNET 2015 data. A more in-depth evaluation of ERA5-Land precipitation data is left for future. We used

177 spline interpolation to derive half-hourly time series from the hourly FLUXNET 2015 data in Tapajos. The half-hourly net

178 radiation time series was used to define daytime hours (i.e. with $S_{net} > 0$) which were set from 6 a.m. to 6 p.m. in Paracou, and

179 from 7 a.m. to 7 p.m. in Tapajos. The dry season was defined as a period with fortnightly rainfall below 50 mm on average

180 across years, consistent with the 100 mm per month used by Bonal et al. (2008). This leads to a 4-month dry season in Paracou

181 (August 1st to December 1st), and a 4.5-month dry season in Tapajos (June 15 to November 1st). Dry seasons were defined

182   for illustration purposes only and have no effect on the model behaviour, which is driven by the meteorological inputs described
183   above.

2.2 Calibration and simulation set-up

185   We calibrated the three forest structure parameters (m, a_{CR} and b_{CR}) for each site. a_{CR} and b_{CR} are not independent, and we used
186   the TALLO global database of crown radius (CR) and diameter (dbh) measurements (Jucker et al., 2022) to infer their
187   relationship. To do so, we restricted the TALLO database to observations located within 10 km around sites from which we
188   generated a thousand pairs of (a_{CR}, b_{CR}) values. Each pair of values was determined by randomly drawing 10 individuals per 10-
189   cm diameter class to generate a size-balanced dataset to which the following model was fitted: $log(CR) \sim N[a_{CR} +$
190    $b_{CR} \times log(dbh), \sigma^2]$. This resulted in the following linear relationship between the two parameters: $b_{CR} = -0.39 +$
191    $0.59 \times a_{CR} + \epsilon_{b_{CR}}$, with $\epsilon_{b_{CR}}$ the error around the relation. This relationship constrained the exploration of the three-
192   dimensional parameter space, so we only had to calibrate a_{CR}, $\epsilon_{b_{CR}}$, and m. Based on preliminary exploratory analyses with
193   the previous version of TROLL, we defined the range of calibration for each parameter and site as follows: a_{CR} varied from
194   1.60 to 2.00 in Paracou and from 2.3 to 2.7 in Tapajos with a step of 0.05, $\epsilon_{b_{CR}}$ from -0.30 to 0.10 in both sites with a step of
195   0.05, and m from 0.030 to 0.050 in both sites with a step of 0.0025. This resulted in $9\ a_{CR} \times 5\ \epsilon_{b_{CR}} \times 9\ m \times 2\ site = 810$
196   triplets of parameter values.

198   For each set of three parameter values, we performed a 600-year simulation from bare ground over a 4-ha area. Simulations
199   were run with an external seed rain uniformly distributed across species, so that the simulated community structure is an
200   emergent property resulting from the community assembly mechanisms embedded in the model. As succession unfolds and
201   the number of mature trees increases in the simulation, internal seed production increases according to the assumed
202   relationships between individual size and fecundity. An alternative to uniform seed rain across species would be to prescribe
203   non-uniform seed rain based on species' regional abundances. This approach would tend to make the simulated species
204   abundances more closely resemble the observed regional abundances. In contrast, uniform seed rain as simulated here, biases
205   the simulated abundances towards evenness across species, and differences in simulated abundances reflect differences in
206   demographic performance controlled by the model trait-based parameterization rather than prescribed differences in the seed
207   rain. Each simulation was forced each year by randomly drawing a year among the ten years of climatic data. In doing so, we
208   avoided applying a periodic climatic forcing or any potential trend linked to global warming.

210   To evaluate the forest structure simulated with each triplet of parameter values, we compared simulated to observed total
211   aboveground biomass (AGB^{tot}, Mg ha^{-1}), total tree abundance (N^{tot}, ha^{-1}), and tree abundances per 5-cm diameter class (N^i, ha^{-1}
212   for dbh class i) at the end of the 600-year regeneration. The Paracou reference dataset was a 2015 inventory of trees with dbh
213   >10 cm in six 6-ha plots (Derroire et al., 2023). The Tapajos reference dataset was a 1999 inventory of trees with dbh > 10 cm

8

214 in 19.75 ha along four 1-km transects (Rice et al., 2004). At both sites, we calculated the relative root mean squared error

215 defined as:

$$RRMSEP = \frac{AGB^{tot}_o - AGB^{tot}_s}{AGB^{tot}_o} + \frac{N^{tot}_o - N^{tot}_s}{N^{tot}_o} + \frac{\sqrt{\frac{1}{n} \times \sum_{i=1}^{n} (N^i_o - N^i_s)^2}}{|N^i_o|}$$

218 where AGB^{tot}_o, N^{tot}_o and N^i_o are observed values, and AGB^{tot}_s, N^{tot}_s and N^i_s are the simulated values. n is the number of dbh

219 classes and $|N^i_o|$ is the mean tree abundances among dbh classes. We extracted the simulation with the lowest $RRMSEP$ at each

220 site and used the corresponding values for m, a_{CR} and b_{CR} in all subsequent simulations.

222 After 600 simulated years of forest dynamics the system reached a mature forest stage with stable forest structure, composition,

223 and functioning at both sites. This is referred to as the 'spin-up phase'. We then used this mature forest stage to calibrate the

224 three parameters of the phenological module. We performed an exhaustive search in the parameter space for combinations of

225 $a_{T,o}$ in [0.01, 0.025, 0.05, 0.075, 0.1, 0.2, 0.3, 0.4, 0.5], $b_{T,o}$ in [0.01, 0.015, 0.02, 0.05, 0.04, 0.06, 0.08, 0.10], and δ_o in [0.1,

226 0.2, 0.3, 0.4, 0.5] resulting in $9\ a_{T,o} \times 8\ b_{T,o} \times 5\ \delta_o \times 2\ sites = 720$ simulations. For each triplet, we ran a 20-year

227 simulation with historical weather repeating the 10 years of data twice with the mature forest as an initial condition. Only the

228 last 10 years were used for the calibration to allow the leaf dynamics to adjust to new parameter values.

230 To evaluate each simulation, we used leaf litter data from litter traps at both sites (unpublished data at Paracou, Rice et al.,

231 2008 at Tapajos). Litter traps were typically collected fortnightly (although time intervals between consecutive litter trap

232 collections were sometimes higher and up to 80 days in Paracou) between 2004 and 2023 in Paracou, and between 2000 and

233 2005 in Tapajos. The litter collected from the traps was oven-dried until the mass stabilised, partitioned between leaves, fruits

234 and woody debris, and then the fraction were weighed. We computed observed leaf litterfall flux in Mg ha^{-1} year^{-1} as the mean

235 across traps converted from trap surface to hectare and time interval in days to year. We also recorded the time interval between

236 consecutive trap collections to account for the smoothing effect of the longer time intervals in simulated data. Simulated leaf

237 litterfall fluxes over the last 10 years of simulation for each triplet of parameter values were compared to the observed fluxes

238 using the same observation dates and corresponding time intervals.

240 To compare simulations against observations, we defined two yearly indices that quantify the timing and intensity of the

241 litterfall peak. The two indices are (i) the day of the litterfall peak as the Julian day of the maximum annual litterfall flux value

242 (*day*), and (ii) the ratio between the maximum value (computed as the average of litterfall flux over the two consecutive time

243 intervals before and after the peak day) divided by the basal flux (computed as the yearly average between January and April)

244 (*ratio*). Both indices are key features of litterfall patterns in tropical rainforests (Chave et al., 2010; Yang et al., 2021). For

245 each simulation we calculated the root mean squared error defined as:

246
$$RMSEP = \sqrt{\frac{\sum_{y=y_0}^{y=y_{max}} (ratio_{y,o} - ratio_{y,s})^2}{N_{year}} + \frac{\sum_{y=y_0}^{y=y_{max}} (day_{y,o} - day_{y,s})^2}{N_{year}}}$$

247 where $day_{y,o}$ and $ratio_{y,o}$ are observed z-scores (i.e., standard deviations from the mean) for year y, and $day_{y,s}$ and $ratio_{y,s}$ are

248 simulated z-scores for year y. Thus a unit *RMSEP* corresponds to a ratio error of one standard deviation, *i.e.* 7.6 folds, or to a

249 day error of one standard deviation, *i.e.* 45.5 days. The best-fit parameters were those corresponding to the lowest *RMSEP* at

250 each site.

251

252 Finally, to quantify the envelopes of stochastic simulation outputs, we ran ten replicates of 600-year simulations starting from

253 bare ground with the six calibrated parameter values.

254 **2.3 Evaluation of forest structure and composition**

255 To assess the model's ability to simulate forest structure, species and functional composition, we used airborne lidar scanning

256 (ALS) and satellite data, as well as forest inventories combined with functional traits. Independently from the calibration, we

257 evaluated the diameter distribution of the forest understory at Paracou using an independent 9-ha inventory of trees with dbh

258 between 1 and 10 cm from 2020-2023 (unpublished data). We evaluated the structure of the simulated forest at the end of the

259 600-year replicates against observed basal area (BA, $m^2\,ha^{-1}$) and logarithm of tree abundance (ha^{-1}) per 1-cm diameter class

260 below 10 cm. We evaluated tree height distributions using ALS data from 2015 at Paracou (unpublished data) and from 2012

261 at Tapajos (dos-Santos et al., 2019), which were processed into canopy height models with a standardised pipeline (Fischer et

262 al., 2024). From both simulated and ALS-derived canopy height models, we derived the distribution of canopy height,

263 expressed in proportion of 1-m^2 pixels per 1-m height class. We evaluated the species composition after the 600-year replicates

264 against the observed rank-abundance curve of the 114 most abundant species at both sites, and the functional composition

265 against the observed density distribution of each trait for each site and each plot. Due to a lower taxonomic resolution of

266 botanical identification at the Tapajos site, we used genus level functional trait data at Tapajos and species level functional trait

267 data at Paracou.

268 **2.4 Evaluation of total leaf area dynamics**

269 We assessed the model's ability to represent the dynamics of total leaf area and its partitioning into three leaf age cohorts

270 (Maréchaux et al., submitted companion paper). For evaluation, we gathered leaf area index (LAI) datasets as follows: LAI

271 from MODIS satellites at both sites, LAI from terrestrial lidar at Tapajos (Smith et al., 2019), and LAI from UAV-borne lidar

272 at Paracou (unpublished data; Vincent et al., 2017). The MODIS LAI product was at 8 day and 500 m resolution, and pre-

273 processed in PLUMBER2 (Ukkoloa et al., 2020). At Tapajos, plant area index (PAI) was derived from terrestrial lidar scanning

274 (TLS) performed every 1-2 months in 2010, 2012, 2015 and 2017 along four 1-km long transects representing 0.4 ha with a

275 spatial resolution of about 3 m to characterise canopy porosity (Smith et al., 2019). PAI was derived from lidar hits following

276 Stark et al. (2012) and based on the MacArthur–Horn transformation (MacArthur & Horn, 1969). This PAI was then converted

277 to LAI using an annual mean LAI of 5.7 (Stark et al., 2012). In Paracou, the PAI was derived from repeated UAV-borne lidar

278 surveys, resulting in PAI mapping at 21 day and 1 m resolution between 2020 and 2022 over a 2.5 ha forest area. This PAI

279 derived from UAV lidar was obtained by vertical integration of Plant Area Density (PAD) profiles previously recalibrated to

280 match a TLS-derived PAD profile of a common 1-ha plot scanned in October 2019. This was required because the limited

281 penetration of the UAV lidar yielded overestimation of raw PAD values (Vincent et al., 2023). This PAI was converted to LAI

282 variation with a factor of 0.68, where the conversion factor is derived from other products.

283

284 Simulated LAI variation per leaf age cohort (Eqs 56-57, Maréchaux et al. submitted companion paper) were compared

285 qualitatively against the one derived from phenological cameras by Wu et al., (2016) at Tapajos and from the reanalysis of

286 Yang et al. (2023) at both sites. Wu et al. (2016) analysed 478 images collected over 24 months from 65 tree crowns and fitted

287 the transition from young to mature and from mature to old leaf pools, assumed to occur at 1 and 3 months, respectively. Yang

288 et al. (2023) used global satellite observations of the TROPOMI satellite Solar Induced Fluorescence (SIF) sensor as an

289 indicator of leaf photosynthesis variation, validated by *in situ* measurements, and set the transition from young to mature and

290 from mature to old leaf pools, occuring at 1.71 and 5.14 months, respectively. By comparison, simulated leaf age per cohort

291 depends on the individual leaf lifespan in TROLL 4.0 (see Maréchaux et al. submitted companion paper).

2.5 Evaluation of carbon and water fluxes

293 To assess the model's ability to simulate carbon and water fluxes, we evaluated gross primary productivity (GPP, kgC m^{-2}

294 year^{-1}) and evapotranspiration (ET, mm day^{-1}). We extracted GPP and latent heat flux (LE, W m^{-2} half-hour^{-1}) from the

295 FLUXNET 2015 dataset (Pastorello et al., 2020). ET was derived from LE and temperature (T, in °C) using $ET =$

296 $\frac{LE \times 60 \times 30 \times 10^{-6}}{\lambda(T)}$ $with$ $\lambda(T) = 2.501 - (2.361 \times 10^{-3}) \times T$ (Allen et al., 1998). GPP was obtained from net ecosystem

297 exchange with the nighttime partitioning method (Reichstein et al., 2005). We summarised half-hourly GPP and ET into daily

298 values by calculating the daily mean and sum. TROLL 4.0 carbon fluxes were also compared with a remotely sensed product

299 of GPP derived from TROPOMI SIF using the formula $GPP = 15.343 \times SIF$ (Chen et al. 2022). We compared how the

300 fluxes depended on environmental drivers in both simulated and observed data. Using the FLUXNET 2015 dataset (Pastorello

301 et al., 2020), daily values of cumulative photosynthetically active radiation (PAR, mol m^{-2}), maximum vapour pressure deficit

302 (VPD, kPa), mean temperature (T, °C), and mean wind speed (WS, m s^{-1}) were calculated, and simulated and observed

303 responses of GPP and ET to PAR, VPD, T and WS were compared. TROLL 4.0 water fluxes were assessed using the relative

304 variation of soil water content (RSWC, %) of the top horizon from the Paracou eddy flux tower (Bonal et al., 2008) and the

305 relative variation of soil water content of the top horizon reanalysed against the climatic water deficit at Tapajos (Restrepo-

306 Coupe et al., 2024). RSWC is defined as the daily mean of soil water content (m^3 m^{-3}) divided by the annual 95th quantile of

307 the daily mean.

308

309 All simulations were run using TROLL 4.0 (Maréchaux et al., submitted companion paper) wrapped in the R package *rcontroll*

310 (Schmitt et al., 2023) and encapsulated in a Singularity image (Kurtzer et al., 2017) leveraging a Python Snakemake workflow

311 (Köster et al., 2012) on a high performance computing platform using 100 cores.

3 Results

3.1 Forest structure and composition

314 We calibrated background mortality rate (m) and crown radius scaling parameters (a_{CR} and b_{CR}) at Paracou and Tapajos against

315 observed aboveground biomass, total abundance and abundance per 5-cm dbh classes, and found m=0.035, a_{CR}=1.80 and

316 b_{CR}=0.3860 at Paracou, and m=0.040, a_{CR}=2.45 and b_{CR}=0.7565 at Tapajos. The modelled aboveground biomass, total

317 abundance and abundance per 5-cm dbh classes were in good agreement with observations (correlation coefficient, CC>0.99

318 at both sites, Fig. 1). The three parameter values were very similar across the five best simulations, i.e. the ones minimising

319 RRMSEP (m±0.0025, a_{CR}±0.1 and b_{CR}±0.057 at Paracou and m±0.01, a_{CR}±0.1 and b_{CR}±0.0285 at Tapajos), and we used the

320 values of the best simulation in all subsequent simulations.
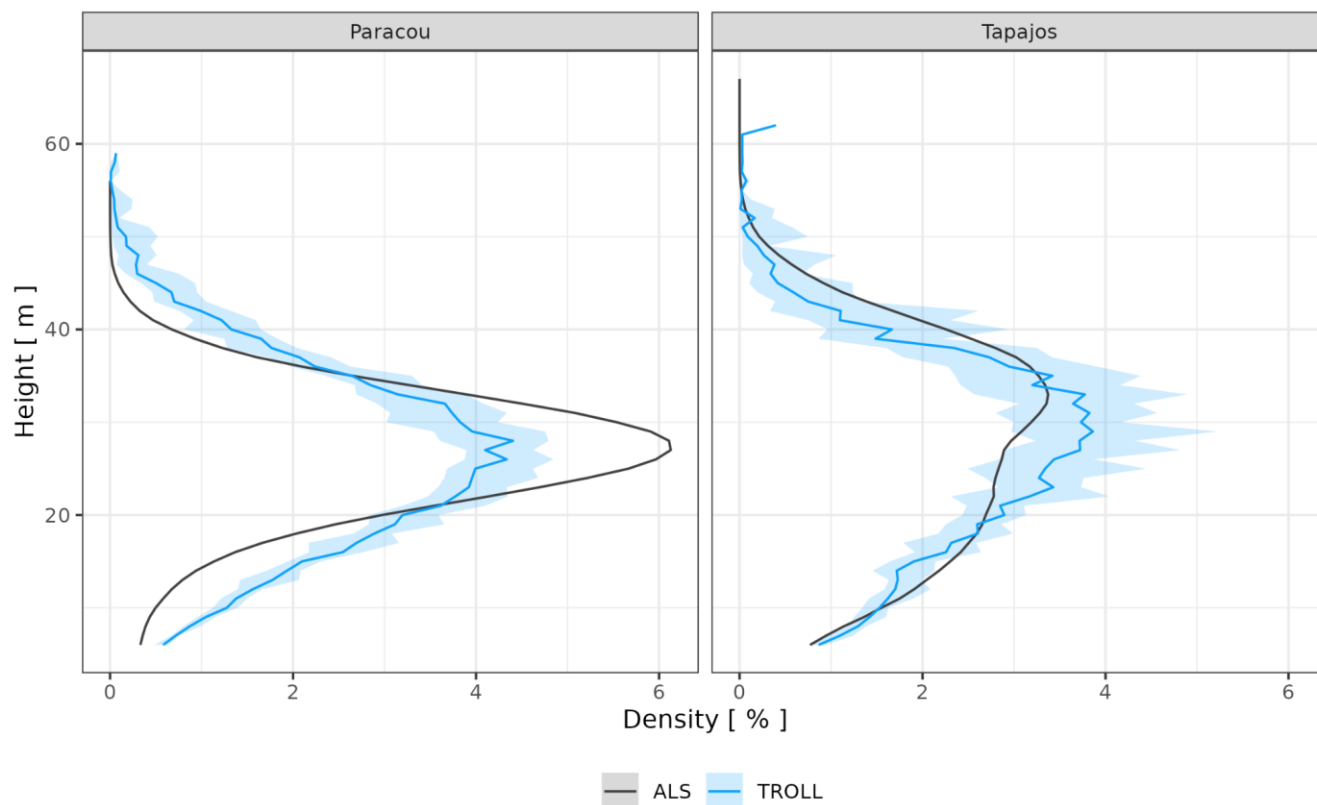
321

322
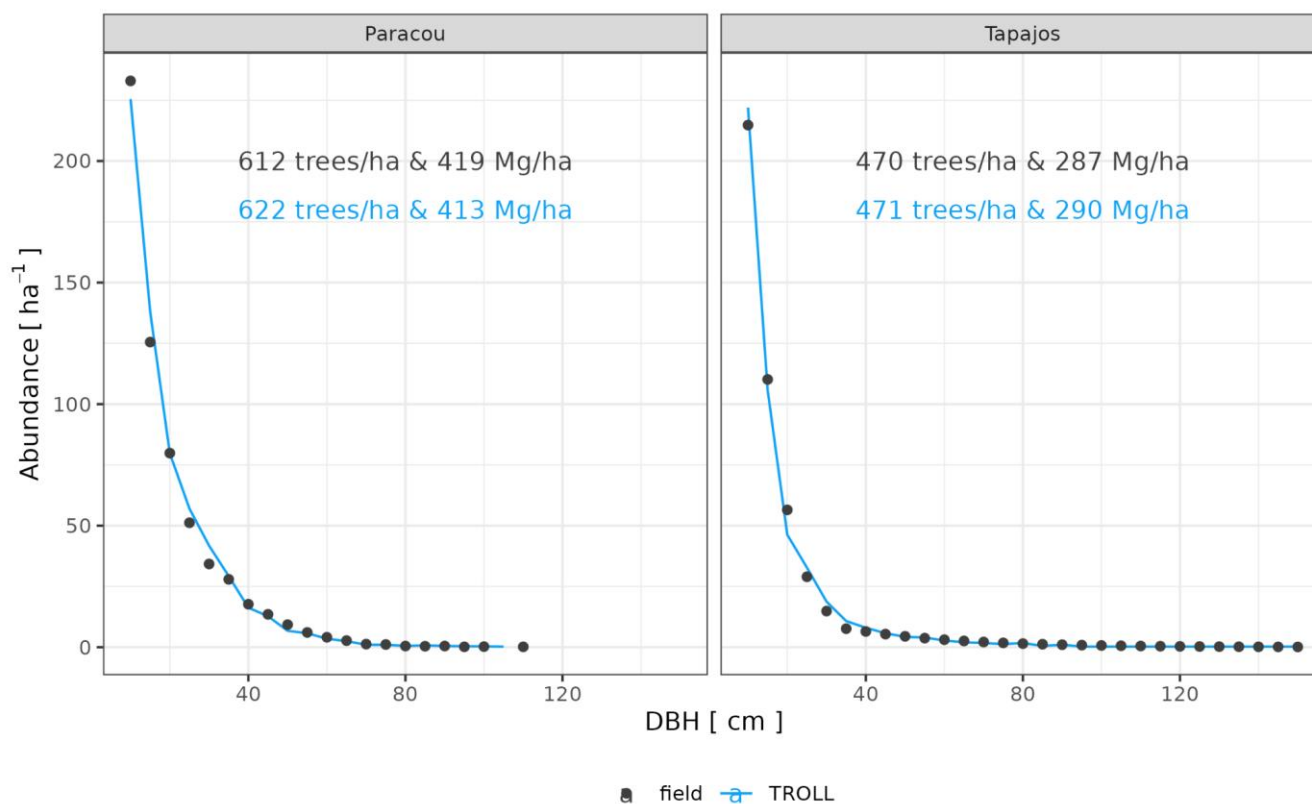
Figure 1: Tree size structure at Paracou and Tapajos, expressed in terms of tree abundances per 5 cm-dbh classes. Comparison between distributions simulated by TROLL 4.0 after calibration of m, a_{CR} and b_{CR} in blue and the ones derived from field inventories of trees with dbh >10 cm in black, at Paracou (left) and Tapajos (right). Observed (black) and simulated (blue) densities of trees with dbh > 10 cm, and aboveground biomass are also provided. All simulated values correspond to the end-state of a 600-year regeneration from bare ground with calibrated values for m, a_{CR} and b_{CR} at each site.

After calibration, the canopy height distribution simulated by TROLL 4.0 matched that measured by lidar aerial scanning (ALS), with a root mean square error of prediction (RMSEP) of the proportion of 1-m² pixels per 1-m height class below 0.8% and a correlation coefficient (CC) above 0.91, despite a slight overestimation of low canopy areas in Paracou, at heights below 20 m, and a slight underestimation of high canopy areas, above 40 m in Tapajos (Fig. 2). For example, in Paracou, 4% of the 1-m² pixels scanned by ALS had a canopy height around 25m. An RMSEP of 0.8% means that TROLL simulations could lead to 3.2 or 4.8% of pixels with a canopy height of 25m. TROLL 4.0 simulations also reproduced the forest understory structure characterised by basal area (BA) and tree abundance distribution per 1-cm diameter classes for trees < 10 cm dbh at Paracou (Fig. 3). However, TROLL 4.0 underestimated the number of small trees (2,139 vs. 3,787 trees ha^{-1}), resulting in an underestimation of basal area (BA = 2.9 vs. 3.7 m²ha^{-1}).


Figure 2: Canopy height distribution at Paracou and Tapajos, expressed in proportion of 1-m² pixels (%) per 1-m height classes. Comparison between distributions derived from a canopy height model simulated by TROLL 4.0 (blue lines), the ones derived from

341 **a canopy height model from airborne laser scanning (black lines). Simulated values and their confidence intervals correspond to the**
342 **end-state of simulations of ten 4-ha 600-year regeneration from bare ground for each site.**
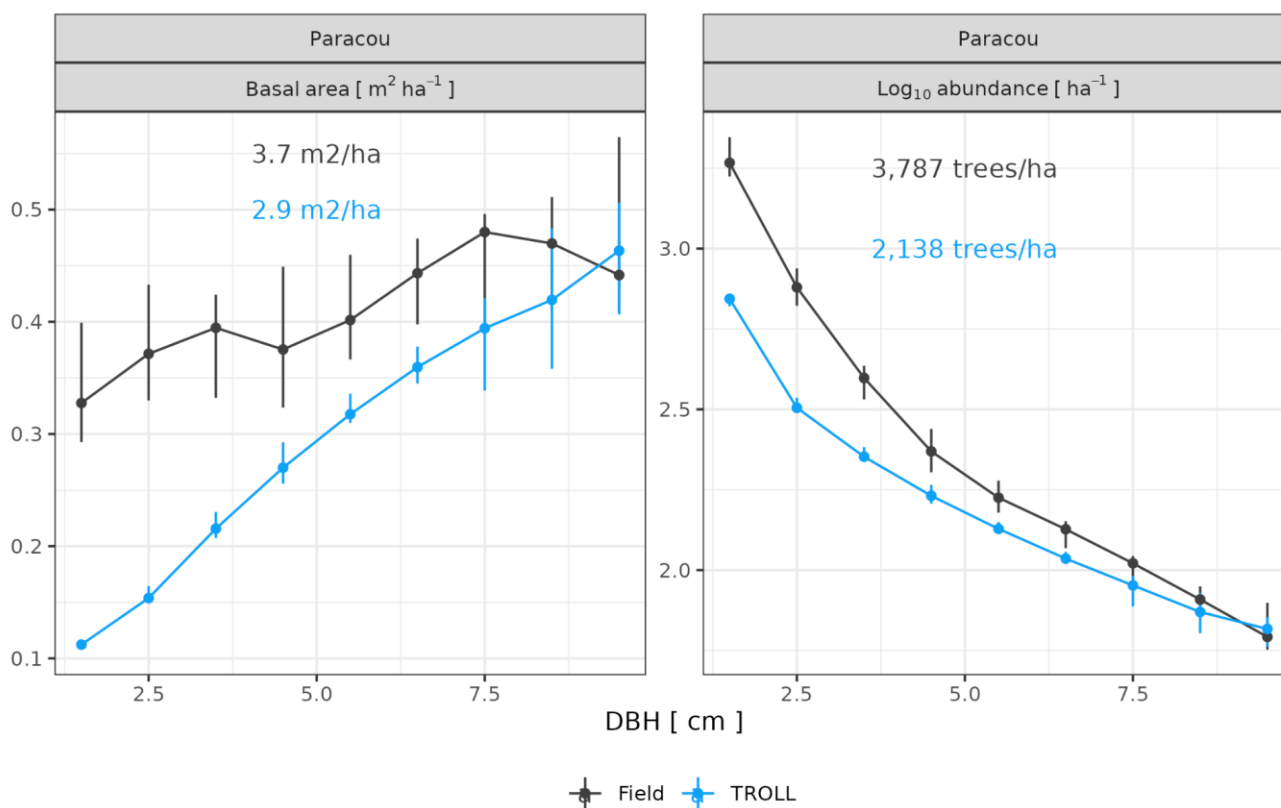
343

344 **Figure 3: Understory tree size structure at Paracou, expressed in terms of basal area distributions (left) and tree abundance (right)**
345 **per 1 cm-dbh classes. The figures compare distributions simulated by TROLL 4.0 in blue and field inventory observations in black.**
346 **Simulated values and their confidence intervals correspond to the end-state of simulations of ten 4-ha 600-year regeneration from**
347 **bare ground. Confidence intervals at 95 % are shown with error bars and are based on variations among plots (9 plots of 1 ha) for**
348 **the observations. Simulated (blue) and observed (black) total basal area (left) and densities (right) for trees with dbh >1 cm and <**
349 **10 cm are also provided. To the best of our knowledge, similar data was not available in Tapajos.**

350 At Paracou, the simulated and observed species rank-abundance curves were similar (Fig. 4), with a RMSEP of 3.67 trees ha⁻

351 ¹ and a CC of 0.93, but with an underestimation in the abundance of dominant species and an overestimation in the

352 abundance of rare species resulting in a higher evenness overall. At Tapajos, the simulated and observed rank-abundance

353 curves displayed similar patterns as at Paracou (RMSEP=3.62 trees ha⁻¹ and CC=0.94) but amplified , with a strong

354 underestimation of the abundance of dominant species and an overestimation of the abundance of rare species.
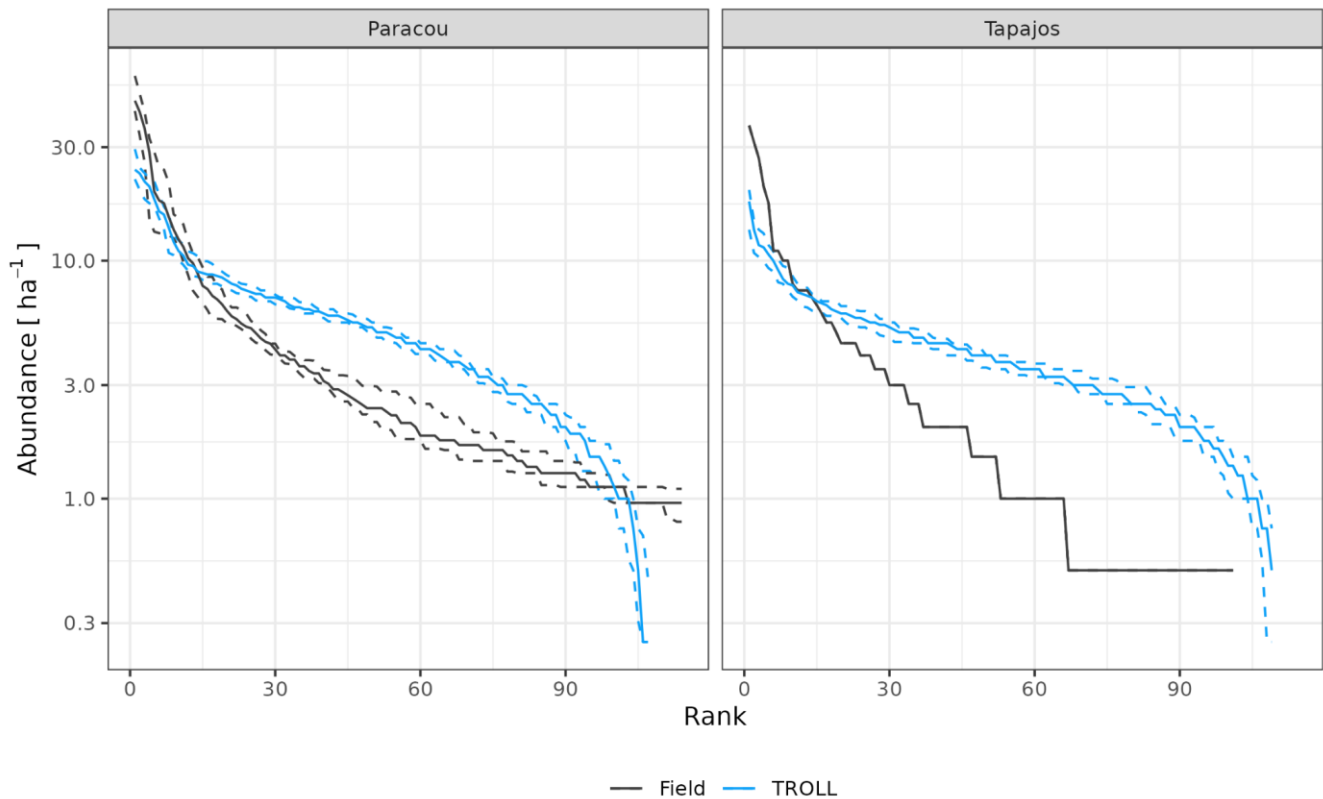
Figure 4: Species-rank abundance curves at Paracou and Tapajos. Comparisons between curves simulated by TROLL 4.0 (blue) and derived from field inventories at both sites. Simulations included 114 and 113 species at Paracou and Tapajos respectively. Curves derived from inventories were cut at the 114th species. Simulated values and their confidence intervals correspond to the end-state of ten 4-ha 600-year regeneration from bare ground. Confidence intervals at 95 % are shown with error bars and are based on variations among plots for observations.

Functional trait distributions simulated by TROLL 4.0 were consistent with empirical ones at Paracou and Tapajos (Fig. 5), with a CC from 0.91 to 1.00 for all traits at both sites, except for leaf area at Paracou (CC=0.74) and Tapajos (CC=0.87). However, abundances of low wood density trees, high LA trees, and high LMA trees were underestimated in simulations when compared to observations at Paracou.
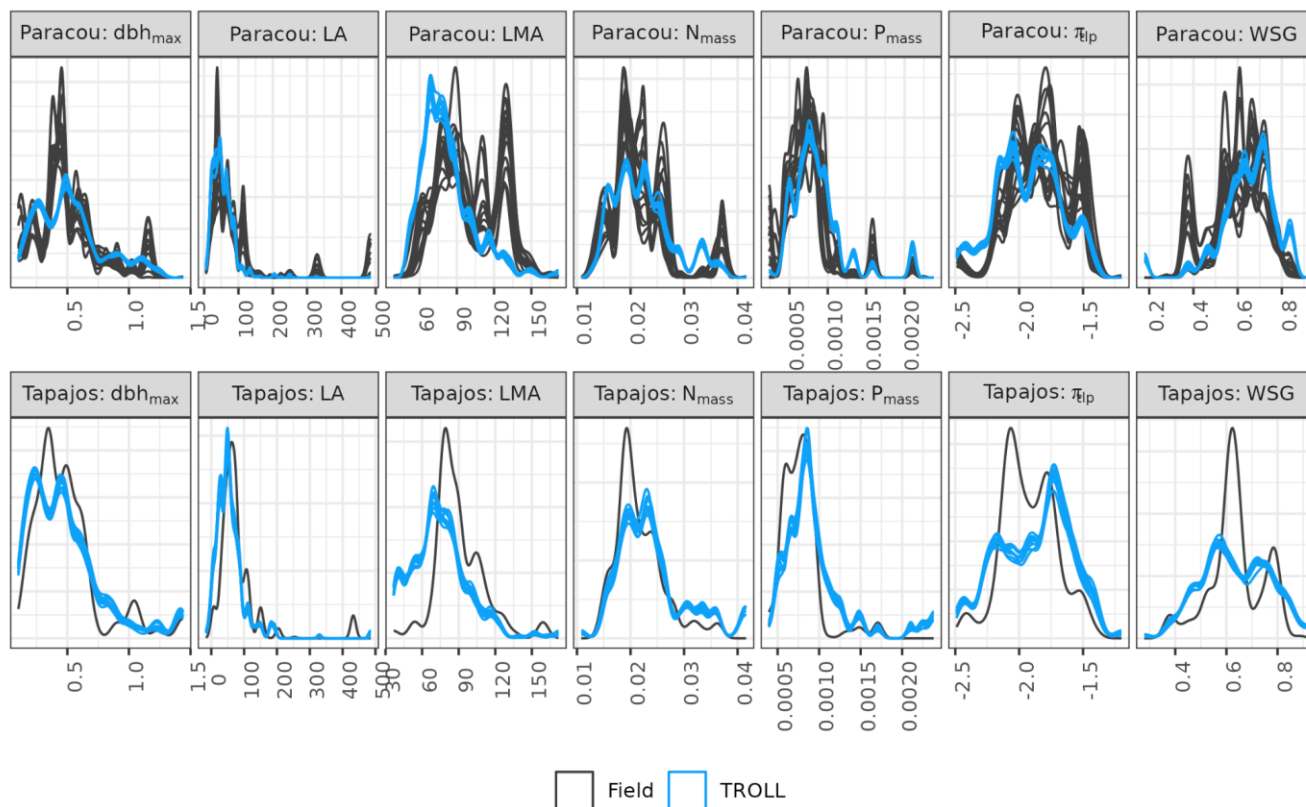
Figure 5: Functional trait distributions at Paracou and Tapajos. Distributions derived from field inventories (black) were based on botanical identification at the species level in Paracou and the genus level in Tapajos. Simulated distributions (blue) were based on the final stage of ten 4-ha 600-year regeneration from bare ground. Confidence intervals are shown with repeated lines and are based on variations among plots for observations and among repetitions for simulations. dbh_{max}: maximum diameter in m, LA: leaf area in cm^2, LMA: leaf mass per area in $g\ cm^{-3}$, N_{mass}: leaf nitrogen content per dry mass in $mg\ g^{-1}$, P_{mass}: leaf phosphorus content per dry mass in $mg\ g^{-1}$, π_{tlp}: leaf water potential at turgor loss point in MPa, WSG: wood specific gravity in $g\ cm^{-3}$.

3.2 Leaf phenology

The calibration of the three parameters of the leaf shedding module against observed litterfall illustrated how each parameter affects the simulated timing and intensity of the litterfall peak during the dry season, with no or little effect on the background litterfall rate (Fig. A2). Calibration resulted in a best-fit $a_{T,o}$ value of 0.2, and a $b_{T,o}$ value of 0.015 at both sites. The calibrated δ_o differed across sites (δ_o=0.1 at Paracou and δ_o=0.2 at Tapajos). The simulated seasonal variation of litterfall at Paracou and Tapajos shows qualitative agreement with the observed data (Fig. 6). Both empirical and simulated data showed a marked peak in litterfall during the dry season, despite a clear under-estimation of simulated litterfall flux during both wet and dry seasons, particularly at Tapajos, and a delayed peak during the dry season, particularly at Paracou, in comparison to observations.
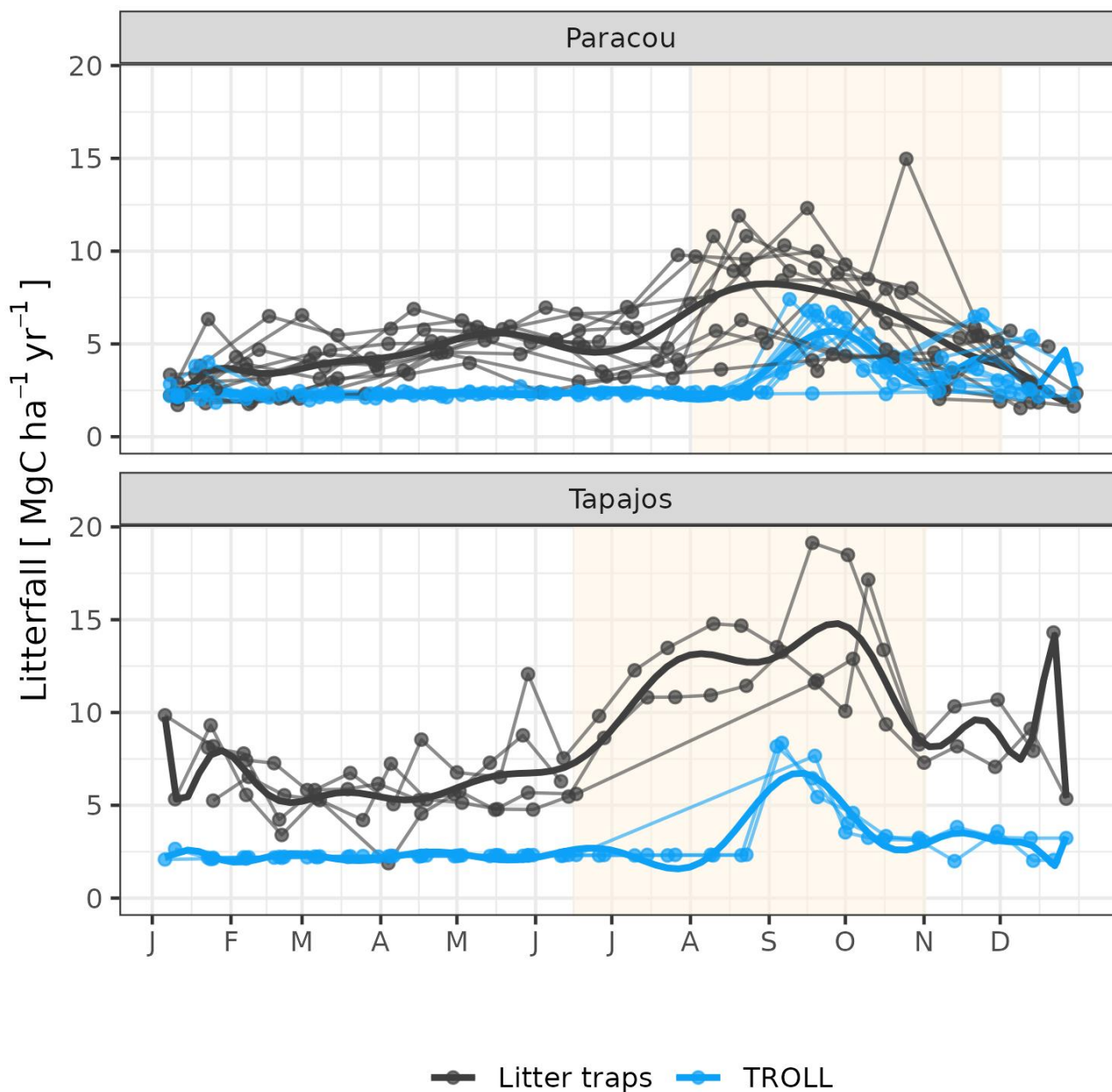
Figure 6: Litterfall annual cycle from fortnightly litterfall fluxes at Paracou and Tapajos. Each thin line represents one year with points showing values at sampling dates, the thick lines represent polynomial smoothing among years, and the vertical yellow bands in the background correspond to the site's climatological dry season. Simulated values correspond to the last 10 years of 20-year simulations starting from the end-state of 600-year regeneration from bare ground with calibrated parameters at each site.

The empirical LAI datasets displayed strikingly different results, illustrating the challenge of estimating LAI with confidence in dense tropical forests (Fig. 7, Tab. A2). MODIS-derived LAI displayed almost no seasonality with mean LAI values

17

389 around 6.0 m² m⁻² at both sites. At Paracou, LAI derived from UAV-borne lidar showed a clear seasonality, with lowest

390 values around 5.5 m² m⁻² from April to June and highest values of almost 6.0 m² m⁻² in December, at the end of the dry

391 season. At Tapajos, LAI derived from terrestrial lidar showed no seasonality, around 5.8 m² m⁻² throughout the year, but LAI

392 derived from phenological cameras (PhenoCams) did display some seasonality, with lowest values at 5.5 m² m⁻² in June and

393 highest values above 6.0 m² m⁻² in December, at the end of the dry season. These observations were compared with

394 simulations. At Paracou, simulated LAI matched the one derived from UAV-borne lidar, both showing an increase during

395 the dry season (CC=0.84, RMSEP=0.11 m² m⁻²). At Tapajos, simulated LAI matched the empirical LAI derived from

396 PhenoCams (CC=0.91, RMSEP=0.15 m² m⁻²; Table A2).

397

398 The different datasets gathered to estimate LAI dynamics per cohorts also showed contrasted patterns (Fig. 8 and Fig. A3).

399 At Tapajos, PhenoCams indicate a maximum young leaf LAI reached during the dry season and a minimum during the wet

400 season, with inverse patterns for old leaf LAI. TROLL 4.0 simulations yielded patterns consistent with these observations

401 (Fig. 8). However, Yang et al.'s (2023) reanalysis predicts the exact opposite trends for young and old leaves, with a

402 maximum young leaf LAI during the wet season and a minimum during the dry season. At Paracou, we could only compare

403 simulated trends against Yang et al. (2023)'s reanalysis and the match was relatively poor (Fig 8).


404
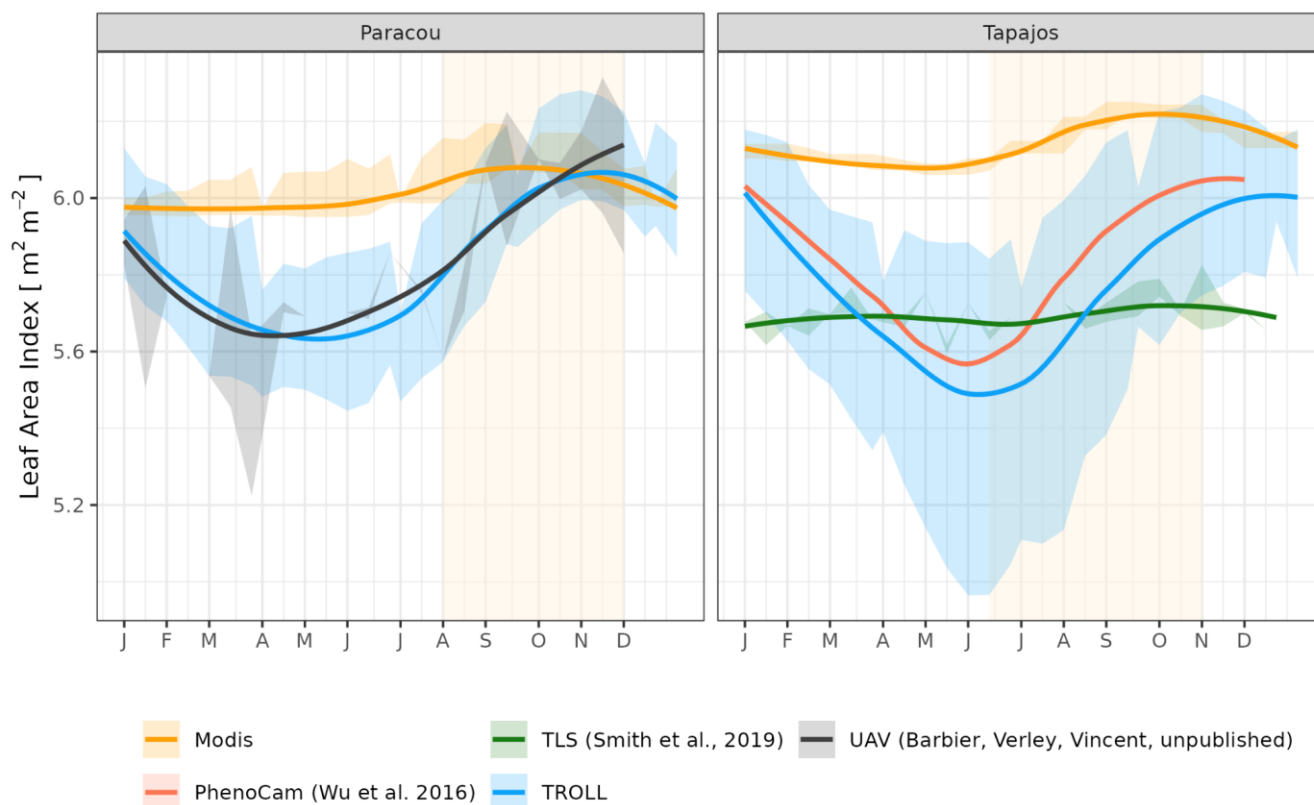
Figure 7: Mean annual cycle of leaf area index (LAI) at Paracou and Tapajos, derived from fortnightly means, from different sources (see methods). Bands are the intervals of means across years, and the vertical yellow bands in the background correspond to the site's climatological dry season. Simulated values correspond to 10 years of simulations starting from the end-state of 600-year regeneration from bare ground with calibrated parameters at each site.
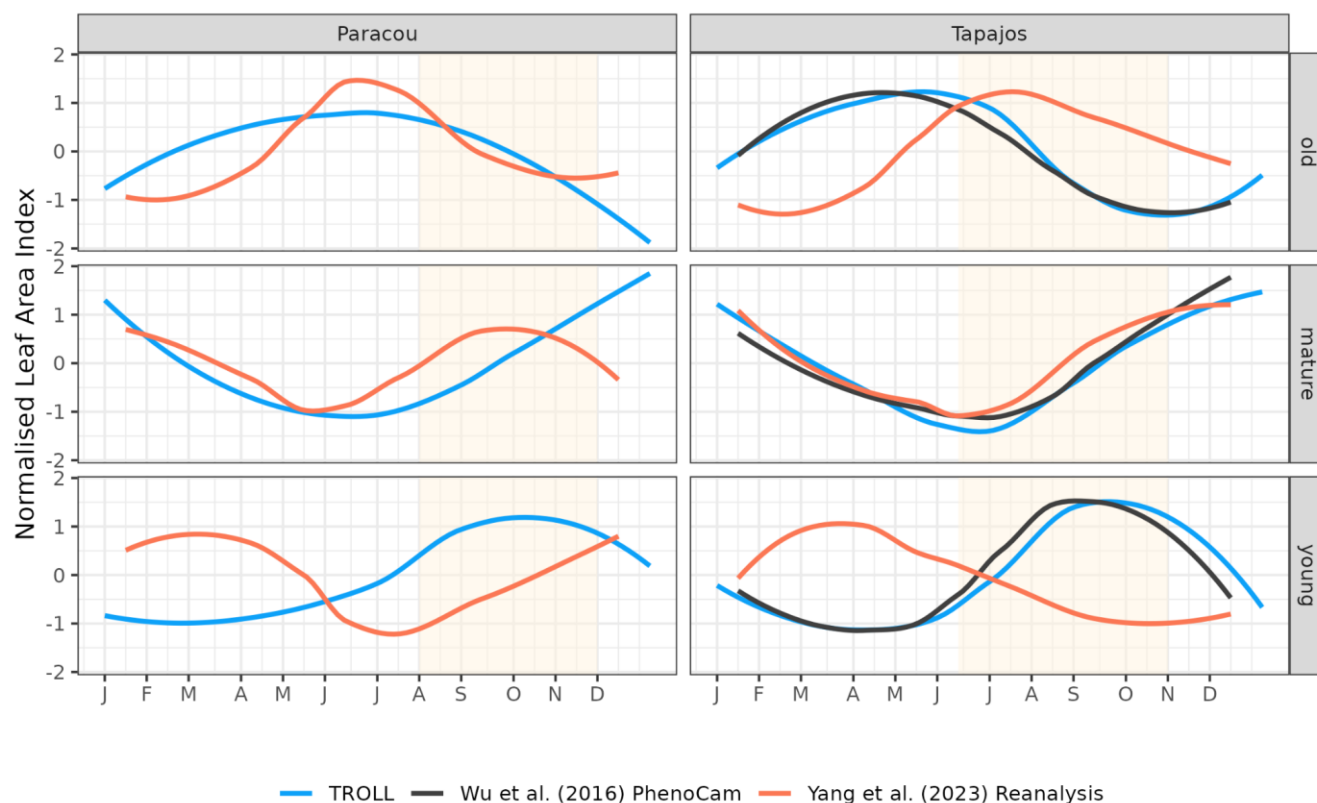
Figure 8: Mean annual cycle of normalised leaf area index per leaf age cohorts, derived from fortnightly means, at Paracou and Tapajos. Note that the three leaf age cohorts (young, mature and old leaves) are not defined the same way in the three sources. Leaf age per cohort depends on the individual leaf lifespan in TROLL 4.0 (see Maréchaux et al., submitted companion paper), while the transition from young to mature and mature to old are respectively fixed to 1.71 and 5.14 months in Yang et al. (2023) and fitted to 1 and 3 months in Wu et al. (2016). The vertical yellow bands in the background correspond to the site's climatological dry season. See figure A3 for absolute variation per cohort, site and dataset. Simulated values correspond to 10 years of simulations starting from the end-state of 600-year regeneration from bare ground with calibrated parameters at each site.

3.3 Water and carbon fluxes

TROLL 4.0 captured the seasonality of gross primary productivity (GPP) observed at the two sites, with an increase before the onset of the dry season, reaching its maximum during the dry season, and a decrease starting before or at the onset of the wet season (Fig. 9 and see Fig. A4 for interannual variations, Tab. A2). Comparison with eddy flux estimates with simulations were high both at Paracou (CC=0.60) and Tapajos (CC=0.46). TROLL 4.0 overestimated GPP at both sites, particularly during the dry season, with a RMSEP of 0.75 and 1.12 kgC m^{-2} year^{-1} when compared with both eddy flux and TROPOMI SIF estimates at Paracou and Tapajos, respectively.
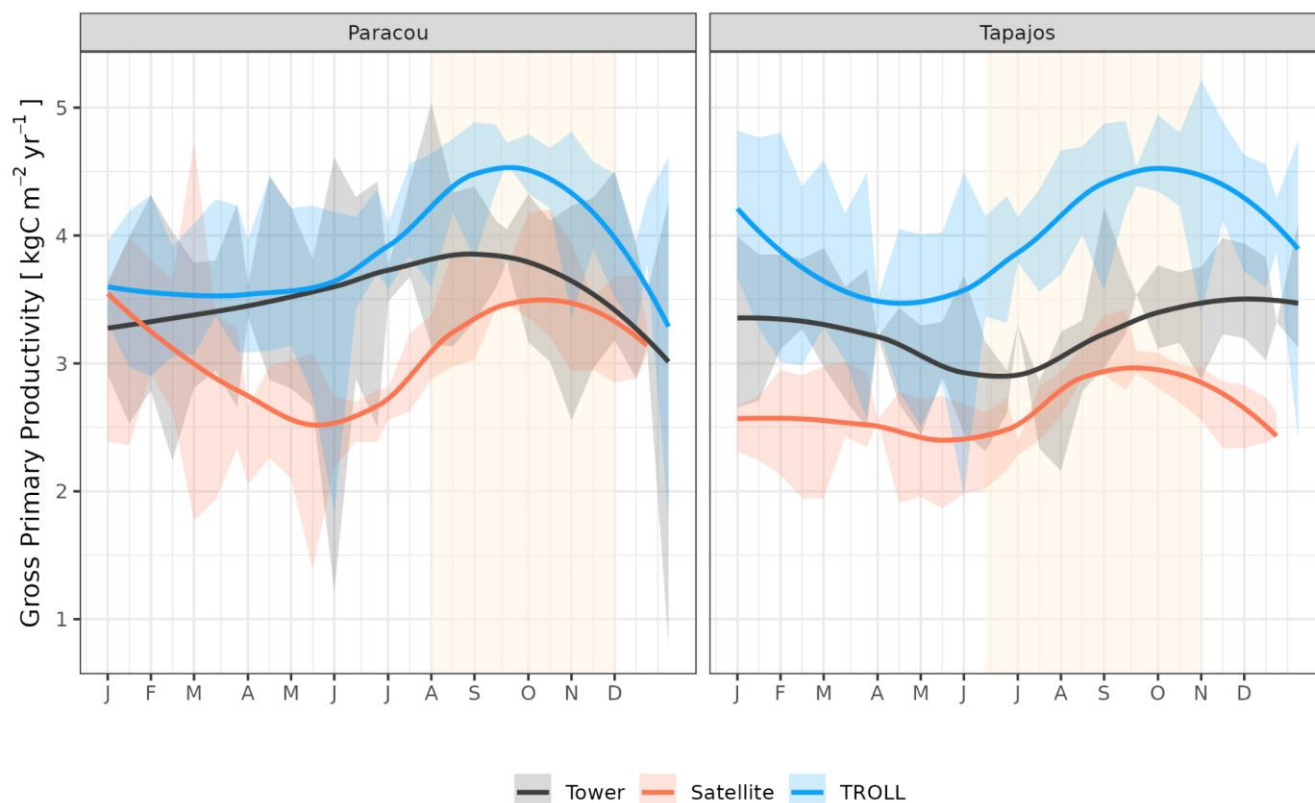
Figure 9: Mean annual cycle of gross primary productivity for Paracou and Tapajos, derived from fortnightly means. The red lines represent the gross primary productivity estimated from TROPOMI SIF while the black lines represent the one derived from eddy flux measurements, and the blue lines the simulated gross primary productivity with TROLL 4.0. Bands are the intervals of means across ten years, and the vertical yellow bands in the background correspond to the site's climatological dry season. Simulated values correspond to 10 years of simulations starting from the end-state of 600-year regeneration from bare ground with calibrated parameters at each site. Inter-annual variations are shown in Figure A4.

The seasonality of water flux was captured by TROLL 4.0 (Fig. 10 and see Fig. A5 for interannual variations, Tab. A2), with a pronounced increase in evapotranspiration (ET) during the dry season at both sites, and leading to CC of 0.66 and 0.70 when compared with eddy flux estimates at Tapajos and Paracou respectively. Although intra-annual variations of simulated and observed values overlapped, TROLL 4.0 tended to overestimate ET in Tapajos during the dry season, leading to RMSEP values of 0.60 and 0.75 mm day^{-1} when compared with eddy flux estimates at Paracou and Tapajos respectively. TROLL 4.0 also captured the seasonality in RSWC of the top soil layer at Paracou and Tapajos (Fig. A6, Table A2, see Fig. A7 for absolute variation with varying depth), with a high RSWC in the wet season close to 100% and a sharp decrease in RSWC in the dry season, although overall smoother in simulations than field estimates.

20
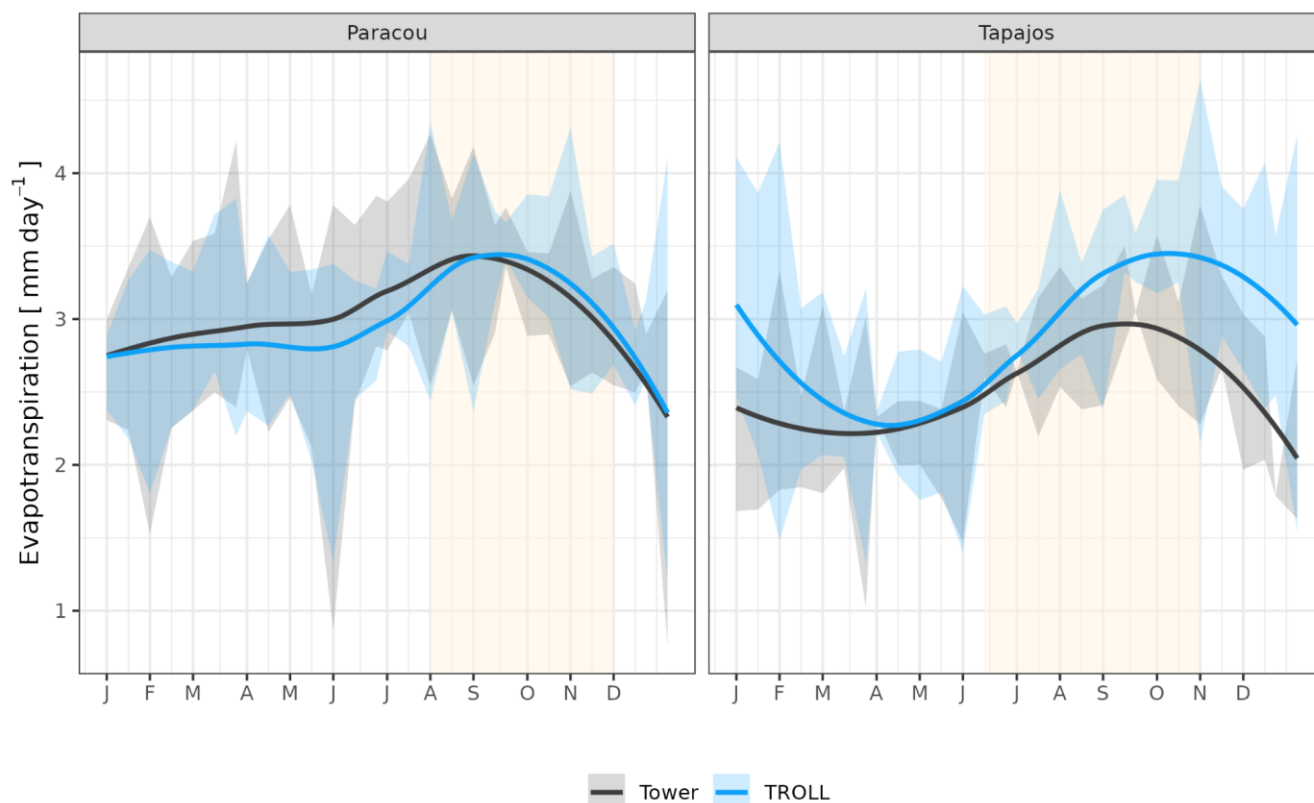
Figure 10: Mean annual cycle of evapotranspiration for Paracou and Tapajos, derived from fortnightly means. The black lines represent the evapotranspiration derived from eddy flux measurements and the blue lines the evapotranspiration simulated with TROLL 4.0. Bands are the intervals of means across years, and the yellow vertical bands in the background correspond to the site's climatological dry season. Simulated values correspond to 10 years of simulations starting from the end-state of 600-year regeneration from bare ground with calibrated parameters at each site. Inter-annual variations are shown in Figure A5.

Both eddy flux-derived and simulated GPP showed a positive logarithmic relationship with cumulative incoming PAR and maximum VPD, and a positive linear relationship with mean temperature at daily scale (Fig. 11). TROLL 4.0 predicted a higher PAR conversion to carbon under high irradiance, high VPD and high temperature conditions when compared to eddy flux estimates, consistent with the higher dry-season GPP in simulations (Fig. 9). Responses of SIF-derived GPP to climatic variables were weak in comparison to simulated and eddy flux derived GPP. Simulated ET was positively correlated with maximum VPD, cumulative PAR and mean temperature, similarly to eddy flux derived ET (Fig. 12). At Paracou, the relationships between environmental drivers and simulated ET, closely aligned with the ones obtained from eddy flux estimates. However, at Tapajos, simulated ET was overestimated under high irradiance, VPD, temperature and windy conditions in comparison to eddy flux estimates. Simulated GPP and ET at both sites were more strongly controlled by environmental variables (higher R^2 in Figs. 11-12) than eddy flux derived GPP and ET.
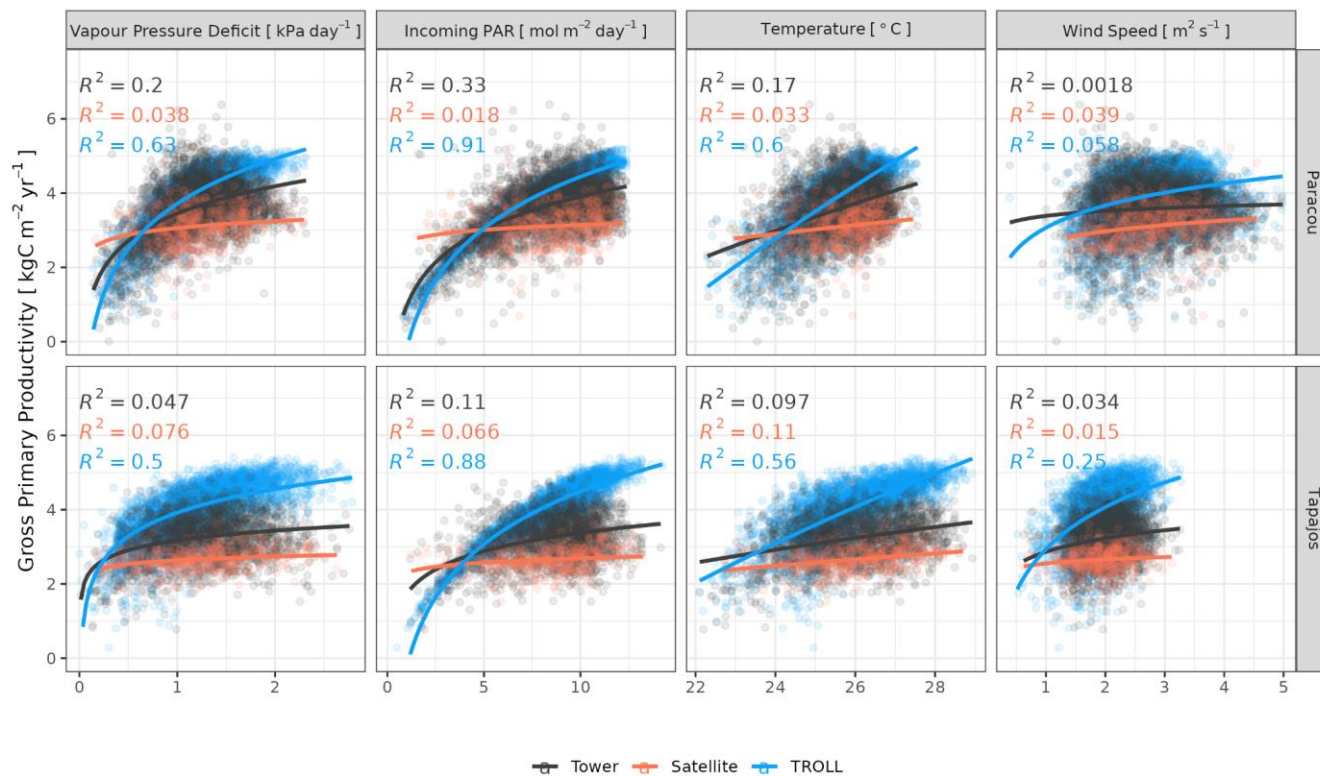
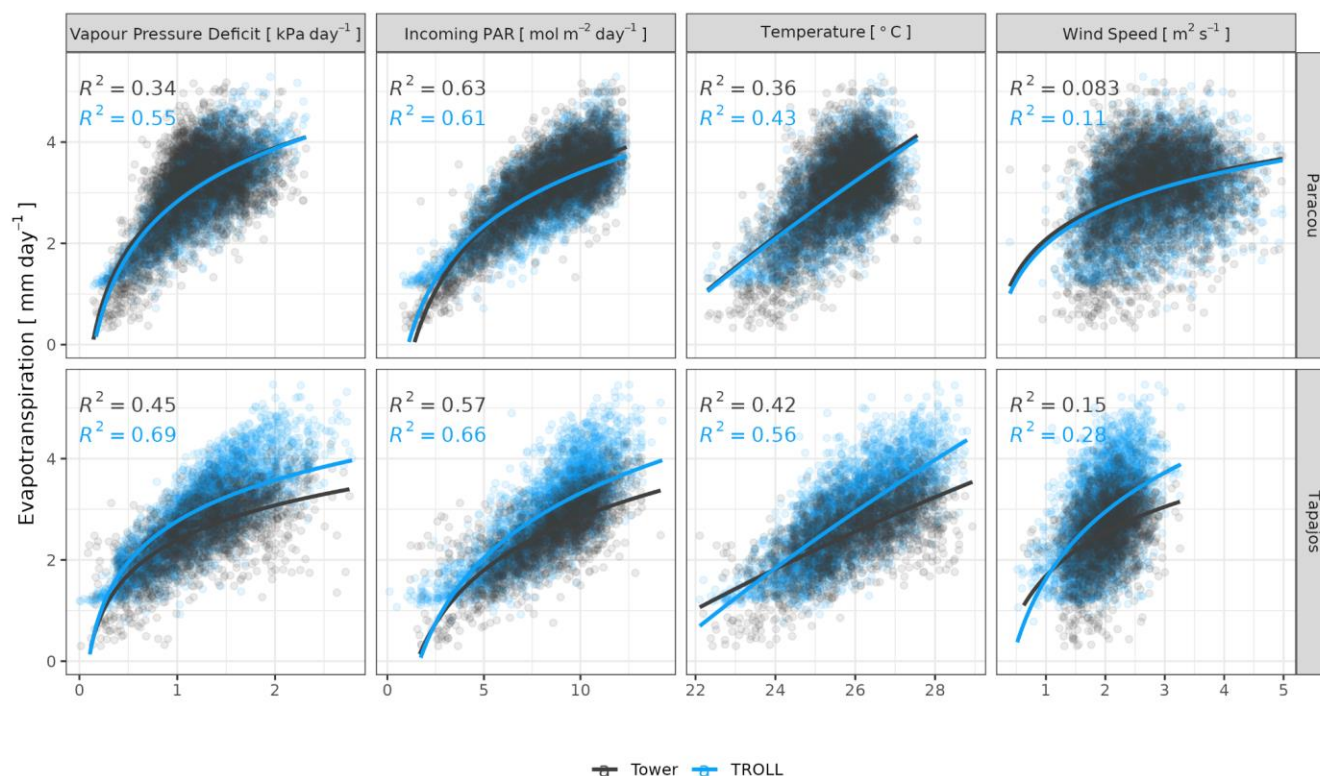**Figure 11: Daily averages of gross primary productivity as a function of daily maximum vapour pressure deficit, total incoming photosynthetically active radiation, average temperature, and average wind speed for model-, satellite- and eddy flux-based estimates at Paracou (top) and Tapajos (bottom). Lines illustrate the linear regression of form y ~ log(x), and text the squared Pearson's R correlation coefficient.**

Figure 12: Daily total evapotranspiration as a function of daily maximum vapour pressure deficit, total incoming photosynthetically active radiation, average temperature, and average wind speed for model- and eddy flux estimates at Paracou and Tapajos. Lines illustrate the linear regression of form y ~ log(x), and text the squared Pearson's R correlation coefficient.

4 Discussion

Here we tested the performance of TROLL 4.0 in reproducing observed forest structure and diversity, but also water and carbon fluxes, and leaf dynamics. We conducted a detailed model evaluation for two Amazonian rainforest sites, Paracou and Tapajos, presenting contrasting climate and soil properties. Both sites have been intensively monitored over the past decades, and we compared the model outputs with available data. We now discuss the consistencies and discrepancies between simulated and observed patterns, potential uncertainties in our results, and the advantages and possible improvements of TROLL 4.0.

4.1 Forest structure and composition

TROLL 4.0 was found to jointly simulate realistic forest structure and species composition (Maréchaux et Chave, 2017). The calibration of three global parameters led to simulated tree abundances across size classes and basal area or aboveground biomass in good agreement with observations from forest inventories. Also, aerial lidar data allowed forest structure to be assessed independently of calibration data. This revealed a good ability of TROLL 4.0 to simulate the horizontal and vertical

477 structure of both forests, which is promising for various applications, including biomass estimation (Knapp et al., 2018).

478 Understory inventories at Paracou also allowed us to independently evaluate TROLL 4.0's ability to simulate tree community

479 structure in the 1 to 10-cm tree diameter range. TROLL 4.0 simulated the distribution of smaller trees reasonably well, although

480 it underestimated individuals from the smallest cohorts. This underestimation of the density of small trees may be partly

481 explained by the fact that the one-metre resolution of the voxel grid used in TROLL 4.0 only allows for one tree per square

482 metre of ground, whereas smaller trees may be squeezed into certain areas of the understorey. However the number of

483 simulated small stems remains lower than the maximal potential number in simulations. Another explanation could be the lack

484 of light heterogeneity in the understorey in simulations in comparison to observations (Montgomery and Chazdon, 2001), thus

485 limiting the opportunities for recruitment of small stems. Explorations of simulated micro-environmental variations within the

486 canopy (de Frenne et al., 2019) and inclusion of trait ontogenetic shifts (Fortunel et al., 2019) could further help understand

487 and improve TROLL's ability to simulate forest structure in the understory.

488

489 TROLL 4.0 attributes individual trees to botanical species and it permits tree functional traits to vary within species. It thus

490 provides a finer-grained description of biodiversity compared to models based on plant functional types (e.g. Longo et al.,

491 2018), and uses a description matching the one of ecologists, in contrast with taxonomy-free continuous trait spectrum

492 approaches (e.g. Sakschewski et al., 2015). The simulated species composition presented classically observed L-shaped profile

493 of species rank abundance distribution in the two sites, but with an over-estimated species evenness resulting in under-abundant

494 dominant species and over-abundant rare species, as already observed in previous versions of the model (Maréchaux and

495 Chave, 2017). Several simulation factors could have resulted in the overestimation of species evenness. The species trait values

496 were extracted from global databases and partially imputed and may therefore not represent the true trait values for the region

497 concerned, which could affect the behaviour of individual species in the model. However, as this noise is random, it seems

498 unlikely that the global values and imputation have led to the skewed species abundance. More likely, the simulations used an

499 external seed rain representing immigration from a continuous forest matrix. We here implemented a homogeneous seed rain,

500 in which all species are equally-abundant, as a conservative test of the model's ability to represent community assembly. Here,

501 the simulated composition after regeneration from bare ground is determined by species traits and their simulated effect on

502 demographic processes and species fitness, rather than prescribed differences in seed rain. However, this homogeneous, and

503 therefore unrealistic, seed rain maintains diversity in the simulated forest with a rescue effect, and can dampen species

504 dominance by promoting less dominant species through a high immigration. The effects of the representation of seed

505 production, dispersal and recruitment on simulated communities should be further explored in the future, especially for

506 projections under disturbance scenarios where forest regeneration is key (Diaz-Yanez et al., 2024, Hanbury-Brown et al.,

507 2022).

508

509 TROLL 4.0 also explicitly simulates forest functional diversity in the community. Simulated functional trait distributions

510 matched well the observed distributions at both sites, as already observed in previous versions of the model (Maréchaux and

511 Chave, 2017). In Paracou, the main discrepancies were the lack of individuals with high LMA (between 120 and 150 g m^{-2}),

24

512 low wood specific gravity (below 0.4 g cm^{-3}) and/or high leaf area (above 100 cm^2). In contrast, in Tapajos, the model tended
513 to simulate lower LMA and less negative turgor loss points on average. Since trait combinations are structured at the species
514 level, and trait integration is high dimensional in tropical forests, with decoupled leaf and wood economic spectra (Baraloto et
515 al., 2010) and weak associations between leaf turgor loss point and other leaf traits (Maréchaux et al., 2019), these
516 discrepancies can be more easily interpreted at Paracou where the trait distributions are built on species-level (and not genus-
517 level) information. Regarding the lack of high LMA individuals, TROLL 4.0 underestimated the abundance of common species
518 such as *Lecythis persistens* or *Licania alba*, which present high LMA. These species come from genera that are hyperdominant
519 across the Amazon basin (ter Steege et al., 2013) but may be underrepresented in the simulations due to the overestimation of
520 species evenness in TROLL 4.0 as discussed above. The lack of light wood and high leaf area individuals can be related to the
521 underestimated abundances of light demanding and pioneer species with fast growth (Chave et al., 2009), such as the ones of
522 the genus *Cecropia*. These species are known to quickly colonise forest gaps under high light conditions, thanks to fast carbon
523 assimilation and growth, and the dispersal of a high number of small, potentially dormant, seeds, leading to an omnipresence
524 of these species in the forest seed bank (Holthuijzen and Boerboom, 1982; Alvarez-Buylla and Martínez-Ramos, 1990). In
525 TROLL 4.0, the seed-size mediated tolerance-fecundity trade-off (Muller-Landau et al., 2010) is assumed to be perfectly
526 equalising, and all species present in the local seed bank and able to strive under the local light availability have the same
527 probability of being   recruited per seed. However, this assumption likely disadvantages gap-affiliated species with a
528 colonisation strategy, and could easily be revisited in future model developments.

4.2 Leaf phenology

530 We calibrated and evaluated the new phenology module of TROLL 4.0. The calibration of the three module parameters ($a_{T,o}$,
531 $b_{T,o}$ and δ_o), which together control the variation of old leaf fall under drying conditions, was conducted using litterfall trap
532 data. This resulted in a realistic litterfall seasonality with a peak during the dry season as already documented (Manoli et al.,
533 2018, Chave et al., 2010, van Langenhove et al., 2020). Interestingly, the calibration resulted in the same values for two
534 parameters at the two sites ($a_{T,o}$, $b_{T,o}$) and close values for the third one (δ_o) to which the simulated litterfall pattern is less
535 sensitive (Fig. A2). At both sites, simulations with the mean value of the third parameter resulted in similar evaluations (not
536 shown). This suggests a good transferability of the phenology module across sites without the need for site-specific calibration,
537 although this remains to be further tested at additional sites and in contrasted conditions (e.g. Restrepo-Coupe et al., 2017). A
538 faster shedding of old leaves was assumed to depend on soil water potential in the root zone, rather than soil water content, on
539 individual leaf water potential at turgor loss point, and on tree size. These are biologically reasonable hypotheses and this
540 supports a good generality of the module. However, the current implementation of leaf dynamics in TROLL 4.0 leads to an
541 underestimation of the flux of litterfall in wet and dry seasons and, as a result, of total annual litterfall at both sites. In TROLL
542 4.0, leaf lifespan was parameterized based on an empirical relationship with leaf structure (leaf mass per area; Maréchaux et
543 al., companion paper). Previous relationships provided in the literature (Reich et al., 1991; Reich et al., 1997; Wright et al.,
544 2004) provided contrasting leaf lifespan estimates, with the one implemented in TROLL 4.0 providing among the highest
545 values, calling for a more in-depth exploration of the reliability and transferability of these empirical relationship. Alternative

546 representations, such as the ones based on optimality principles (Kikuzawa 1991, Franklin et al., 2020, Manzoni et al., 2015),

547 and their combination with the environmentally-driven old leaf shedding acceleration implemented in the new module could

548 be explored in the future.

549

550 The evaluation of leaf area index (LAI) and its dynamics was difficult due to the number of products that yield inconsistent

551 time series. Remotely sensed MODIS LAI showed a very small seasonal variation with a slight increase of LAI starting at the

552 beginning of the dry season at both sites. However, MODIS LAI data products are known to be susceptible to the uncertainty

553 affecting the bidirectional reflectance, and to saturate at high LAI values (Petri and Galvão, 2019). Local measurements of

554 LAI through UAV-borne lidar in Paracou showed a stronger increase of total LAI of 0.5 m^2 m^{-2} starting at the beginning of

555 the dry season, and leading to a maximum in the dry season. This pattern of variation was in strong agreement with that

556 simulated for LAI by TROLL 4.0. Similarly, local measurements of top canopy LAI derived from phenological cameras in

557 Tapajos (Wu et al., 2016) also showed a high increase of total LAI in the dry season, above 0.5 m^2 m^{-2}, also in good agreement

558 with the seasonal LAI variation simulated by TROLL 4.0 at that site. By contrast, the LAI derived from terrestrial vertical

559 lidar in Tapajos showed almost no variations (Smith et al., 2019), and such differences with both the patterns derived from

560 phenological cameras and simulations need to be further scrutinised. Among potential explanations, LAI from TLS in Tapajos

561 was adjusted to the annual mean of 5.7 (Stark et al., 2012), leading to lower absolute variations than what was obtained

562 elsewhere, and used coarse spatial and temporal resolutions over small spatial and temporal extents (see material and methods).

563 The discrepancy with simulated patterns could also be linked to uncertainties in LAI variations in the understory in our

564 simulations. Recent studies have suggested opposite variations in LAI between the canopy and the understorey (Nunes et al.,

565 2022), which should be further explored with TROLL 4.0. Overall, while obtaining a robust estimate of LAI temporal variation

566 in tropical forests remains a challenge (Vincent et al., 2023; Bai et al., 2023), the relative variation of LAI simulated by TROLL

567 4.0 matched the most reliable products at each site, providing an encouraging assessment of this model's ability. Importantly,

568 while total LAI variation remains limited on average within a year in tropical rainforests, this hides important turnover across

569 leaf ages and species, and to ensure robust predictions models should endeavour to represent such turnover and its underlying

570 processes (Wu et al., 2017).

571

572 The dry-season increase in total LAI simulated in TROLL 4.0 corresponds to a rejuvenation of the canopy leaf cover associated

573 with a decrease in the LAI of old leaves at the beginning of the dry season, directly followed by an increase in the LAI of

574 young leaves during the dry season. This turnover is in very good agreement with the one captured by phenological cameras

575 at Tapajos (Wu et al., 2016) and documented in other studies (Yang et al., 2021; Doughty and Goulden, 2008), while the SIF-

576 derived young LAI pattern (Yang et al., 2023) showed an opposite pattern at this site. The main difference in simulated cohorts

577 between the two sites is the continuous dominance of old LAI in Tapajos while mature leaves dominated at the end of the dry

578 season in Paracou. This dominance of older (and less efficient) leaves in Tapajos simulations may be linked to the

579 underestimated litterfall flux and soil water depletion during the dry season at this site. However, the relative proportion of

580 leaf area across the different leaf age pools within and across datasets strongly depends on the definition of the leaf age pools

581 themselves. These pools depend on the individual leaf lifespan in TROLL 4.0 (see section 2.6.2 in Maréchaux et al., submitted

582 companion paper), while the transition from young to mature and mature to old are respectively fixed to 1.71 and 5.14 months

583 in Yang et al. (2023) and fitted to 1 and 3 months in Wu et al. (2016). These contrasting approaches may explain the higher

584 relative importance of old leaves in Wu et al. (2016) compared to Yang et al. (2023) and the intermediate values of TROLL

585 4.0 (Fig. 6). The seasonal dynamics of leaf cohorts remains poorly known in tropical forests and additional high-resolution

586 optical imagery, *e.g.* by drones or phenological cameras, would be extremely useful to better document these patterns.

4.3 Water and carbon fluxes

588 At Tapajos, DGVMs simulated opposite seasonal trends in carbon and water fluxes compared to the observed ones (e.g. Fig.

589 1 in Chen et al., 2020; Fig. 5 in Longo et al., 2019b; Fig. 3 in Restrepo-Coupe et al., 2017). In contrast, TROLL 4.0 showed a

590 good ability to represent the dynamics of both carbon and water fluxes estimated with eddy covariance data. In particular,

591 TROLL 4.0 captures the dry season increase in gross primary productivity (GPP) and evapotranspiration (ET) documented for

592 light-limited forests (Guan et al. 2017, Wagner et al. 2016, Aguilos et al. 2018). Simulated GPP and ET also presented realistic

593 daily responses to environmental drivers, namely vapour pressure deficit (VPD), temperature, incident radiation and wind

594 speed, both in direction and relative magnitude.

595

596 However, at Tapajos, we found that TROLL 4.0 overestimated ET during the dry season in comparison to eddy flux-derived

597 ET values, under high irradiance, high VPD and high temperature. Simulated ET consists in tree transpiration summed over

598 simulated individuals, water evaporation from the topsoil layer, and the direct evaporation of the rainfall intercepted by the

599 canopy (Kunert et al., 2017). TROLL 4.0 may underestimate the stomatal control of transpiration during the dry season at

600 Tapajos. Accordingly, the control of ET by atmospheric conditions in Tapajos was overestimated in simulated data in

601 comparison to observations, suggesting a stronger coupling of vegetation and atmosphere at that site than simulated (de Kauwe

602 et al., 2017). Underestimation of stomatal control can result from the representation of stomatal conductance and its responses

603 to soil water availability. These are active areas of research and alternative representations could be considered in the future

604 (Wolf et al. 2016; Anderegg et al. 2018; Sabot et al., 2022, Lamour et al., 2022; see sections 2.5.2 and 2.5.3 and Appendix B

605 in Maréchaux et al. submitted companion paper). Alternatively, during the dry season, a lack of stomatal control can be due to

606 an overestimation of soil water availability in the model. Soil water content dynamics depend on both the soil depth (Fig. A7)

607 and on the soil hydraulic properties. The two sites are known to present heterogeneity in soil properties but we here performed

608 simulations with homogenous soil properties, both horizontally and vertically. For instance in Paracou, the topsoil layer is

609 sandier than the 15-30 cm layer (Van Langenhove et al., 2021). Although TROLL 4.0 quantitatively captures the soil water

610 depletion observed during the dry season, it appears to underestimate this depletion compared to empirical estimates at both

611 sites (Fig. A6). This underestimation occurs in spite of the agreement between simulated and eddy covariance-derived ET

612 during the dry season in Paracou, and of the higher simulated than eddy-covariance-derived ET during the dry season at

613 Tapajos. Testing the model's sensitivity to soil layer thickness and properties will be important to perform prior to forest

614 projections under drier future conditions and model spatial up-scaling (Meunier et al., 2022). For example, simulations with

615   the ED2 model suggested that forest responses to drier conditions at Tapajos strongly depended on soil texture (Longo et al.,
616   2018). Finally, the greater disagreement between simulated and eddy-covariance-derived ET at Tapajos than Paracou also calls
617   for an in-depth evaluation of the global reanalysis precipitation data at this site. More generally, climate of the Amazon is
618   notoriously challenging for models and it is important to further explore climate forcings in vegetation models.

620   TROLL 4.0 tended to overestimate empirical GPP estimates, particularly during the dry season, in comparison to both eddy
621   covariance- and SIF-derived GPP. GPP is driven by the photosynthetic activity of the canopy, which depends on multiple
622   processes (Diao et al., 2023; Slot et al., 2024) and further work would be needed to precisely discriminate among them, while
623   accounting for eddy covariance uncertainties (Cui and Chui, 2019). Among others, simulated GPP is sensitive to the parameters
624   that control light transmission and absorbance (light extinction coefficient, apparent quantum yield; Maréchaux & Chave,
625   2017). Both are assumed fixed and constant in simulations, but are known to vary with leaf angle distribution and leaf optical
626   properties, depending on micro-environmental conditions and species (Long et al., 1993; Poorter et al., 1995; Meir et al., 2000;
627   Kitajima et al., 2005). Also, the response of leaf-level gas exchanges to soil water availability shows no clear consensus across
628   models (Powell et al, 2013; Trugman et al., 2018), and could be underestimated during the dry season in TROLL 4.0
629   simulations. Simulated GPP was higher than inferred from eddy covariance data, which was itself higher than GPP inferred
630   from SIF satellite data (Chen et al., 2022). The eddy covariance-derived GPP were obtained from the net ecosystem exchanges
631   using the nighttime partitioning method (Reichstein et al., 2005). This method was developed for temperate forests with greater
632   temperature variations than tropical forests, which could therefore bias the empirical estimates. In addition, the eddy flux
633   method has long been reported to underestimate CO_2 fluxes (Baldocchi, 2003; Gao et al., 2019). Similarly, even though solar
634   induced fluorescence offers a great potential for the evaluation or the calibration of seasonal carbon fluxes in vegetation
635   models, especially as the tropics are underrepresented by eddy flux tower networks (Villarreal et Vargas, 2021), current SIF
636   products should be used with care (Marrs et al., 2020).

5 Conclusions

638   Here we evaluated the TROLL 4.0 individual-based forest dynamics model, which is capable of jointly simulating forest
639   structure, diversity and functioning. To this end, we assembled data from forest inventories, eddy flux towers, litterfall traps,
640   UAV-borne and terrestrial lidar, phenological cameras, and satellite products at two Amazonian forest sites and found that
641   TROLL 4.0 was able to realistically simulate the forest structure and composition, water and carbon fluxes, and leaf area
642   dynamics. In using data of different nature and under the control of different processes, we limited the emergence of equi-
643   finality issues (Medlyn et al., 2005), suggesting a good transferability and robustness of TROLL 4.0.

645   Comparison with field inventories, aerial and satellite data confirm TROLL 4.0's ability to realistically simulate the structure
646   and composition of tropical forests, without imposing constraints beyond the species pool and calibrating more than three
647   parameters. Discrepancies between observed and simulated tree abundances in small size classes and abundance of trait values

648 specific to colonising species suggest further developments of regeneration processes are needed, a worthy endeavour in the

649 context of increased disturbance regimes. TROLL 4.0 was further able to simultaneously simulate the seasonality of

650 productivity, evapotranspiration and leaf area in these two light-limited forests, as opposed to many current DGVMs (Chen et

651 al., 2020; Restrepo-Coupe et al., 2017; Longo et al., 2019). The model's ability to simulate ecosystem fluxes is further shown

652 by the responses of carbon and water fluxes to environmental drivers, whose direction and relative importance were well

653 aligned with observations at both sites despite contrasting climate and soil properties. Additionally, the dynamics of total leaf

654 area appeared realistically partitioned into different leaf pools, as shown by the leaf rejuvenation during the dry season in these

655 systems (Wu et al., 2016; Yang et al., 2021). However, further inspection of the leaf area dynamics across the canopy vertical

656 profile would be useful. Also, the model overestimation of productivity and evapotranspiration during the dry season calls for

657 a more in-depth exploration of the model representation of respiration, plant hydraulics (e.g., stomatal control), and soil

658 hydrology.

659

660 Overall, our analyses establish the suitability of TROLL 4.0 for simulating forest structure, diversity and ecosystem functioning

661 in short- and long-term studies of tropical forest dynamics, paving the way for multiple applications (Maréchaux et al., 2021).

662 TROLL 4.0 could thus be used for projections of the effects of climate change on tropical forests, and exploration of the effect

663 of biodiversity on forest resilience to these changes (Sakschewski et al., 2016). Similarly, as TROLL 4.0 retains the species-

664 level taxonomic description, it can also help explore the effects of management practices such as timber production, for which

665 half of tropical forests are designated (Blaser et al., 2011). While the development of TROLL 4.0 will continue, in light of

666 knowledge improvement, novel data collection and identification of uncertainties and discrepancies, we believe it represents

667 a valuable tool for addressing the major challenges tropical forests are currently facing.

Code and data availability

669 The TROLL version 4.0 and further developments are publicly available on GitHub as a C++ standalone at

670 https://github.com/TROLL-code/TROLL or wrapped into an R package at https://github.com/sylvainschmitt/rcontroll/. All the

671 code associated with the analyses described in this paper are available at https://github.com/sylvainschmitt/troll_eval and

672 permanently stored at add a zenodo doi after acceptance with corresponding analyses notebook at

673 https://sylvainschmitt.github.io/troll_eval/. Inventories data for Paracou trees over 10 cm are available through request on the

674 CIRAD dataverse: https://dataverse.cirad.fr/dataverse/paracou. Paracou trees understory trees are available through request,

675 PI: GS, GD, JC. Aerial Lidar Scanning from Paracou are available through request (PI: GV) and from dos-Santos et al. (2019)

676 for Tapajos. Species data are available from Jucker et al., (2022), Maréchaux et al., (2015), Guillemot et al., (2022), Vleminckx

677 et al. (2021), Maréchaux et al., (2019), Nemetschek et al., (2024), Schmitt and Boisseaux (2023), Boisseaux et al., (submitted),

678 Ziegler et al., (2019), Baraloto et al., (2010), and from TRY (Kattge, Bönisch, et al., 2020). Soil data have been collected from

679 Van Langenhove et al., (2021), Silver et al., (2000), Quesada et al., (2010), Sabatier et al., (1997), and Nepstad et al., (2002).

680 Eddy covariance data from Paracou and Tapajos sites are available on FLUXNET at https://fluxnet.fluxdata.org (last access:

681   6   September   2023).   ERA5-Land   data   are   available   on   the   Climate   Data   Store:

682   https://cds.climate.copernicus.eu/cdsapp#!/dataset/reanalysis-era5-land?tab=overview. TROPOMI SIF satellite data are

683   available in Chen et al., (2022). Litterfall data at Tapajos are available online through the Oak Ridge National Laboratory

684   (ORNL) Distributed Active Archive Center (DAAC): https://daac.ornl.gov/LBA/guides/CD10_Litter_Tapajos.html and upon-

685   request at Paracou, PI: DB. MODIS LAI data are available online and were extracted from PLUMBER2 on Research Data

686   Australia: https://researchdata.edu.au/plumber2-forcing-evaluation-surface-models/1656048. Terrestrial LAD data from

687   Tapajos are available in Smith et al., (2019). Lidar PAD data from Paracou are available upon-request, PIs: NB and GV. LAI

688   variations among young, mature and leaf cohorts are available from the reanalysis of Yang et al. (2023) at:

689   https://figshare.com/articles/dataset/Leaf_age-dependent_LAI_seasonality_product_Lad-

690   LAI_over_tropical_and_subtropical_evergreen_broadleaved_forests/21700955/4 and from the phenological camera of Wu et

691   al., (2016) at: https://datadryad.org/stash/dataset/doi:10.5061/dryad.8fb47. Tapajos soil moisture data from Restrepo-Coupe et

692   al. (2024) are available at: https://datadryad.org/stash/dataset/doi:10.5061/dryad.d51c5b08g.

Author contributions

Competing interests

Acknowledgements

Financial support

References

Aguilos, M., Hérault, B., Burban, B., Wagner, F., and Bonal, D.: What drives long-term variations in carbon flux and balance in a tropical rainforest in French Guiana?, Agricultural and Forest Meteorology, 253-254, 114–123, https://doi.org/10.1016/j.agrformet.2018.02.009, 2018.

Allen, R. G., Pereira, L. S., Raes, D., & Smith, M. (1998). Crop evapotranspiration-Guidelines for computing crop water requirements-FAO Irrigation and drainage paper 56. *Fao, Rome*, *300*(9), D05109.

Alvarez-Buylla, E. R. and Martinez-Ramos, M.: Demography and allometry of cecropia obtusifolia, a neotropical pioneer tree - an evaluation of the climax-pioneer paradigm for tropical rain forests, The Journal of Ecology, 80, 275, https://doi.org/10.2307/2261011, 1992.

Aragão, L. E. O. C., Malhi, Y., Metcalfe, D. B., Silva-Espejo, J. E., Jiménez, E., Navarrete, D., Almeida, S., Costa, A. C. L., Salinas, N., Phillips, O. L., Anderson, L. O., Alvarez, E., Baker, T. R., Goncalvez, P. H., Huamán-Ovalle, J., Mamani-Solórzano, M., Meir, P., Monteagudo, A., Patiño, S., Peñuela, M. C., Prieto, A., Quesada, C. A., Rozas-Dávila, A., Rudas, A., Silva Jr., J. A., and Vásquez, R.: Above- and below-ground net primary productivity across ten Amazonian forests on contrasting soils, Biogeosciences, 6, 2759–2778, https://doi.org/10.5194/bg-6-2759-2009, 2009.

BALDOCCHI, D. D.: Assessing the eddy covariance technique for evaluating carbon dioxide exchange rates of ecosystems: past, present and future, Global Change Biology, 9, 479–492, https://doi.org/10.1046/j.1365-2486.2003.00629.x, 2003.

Baraloto, C., Timothy Paine, C. E., Poorter, L., Beauchene, J., Bonal, D., Domenach, A.-M., Hérault, B., Patiño, S., Roggy, J.-C., and Chave, J.: Decoupled leaf and stem economics in rain forest trees, Ecology Letters, 13, 1338–1347, https://doi.org/10.1111/j.1461-0248.2010.01517.x, 2010a.

Baraloto, C., Timothy Paine, C. E., Patiño, S., Bonal, D., Hérault, B., and Chave, J.: Functional trait variation and sampling strategies in species-rich plant communities, Functional Ecology, 24, 208–216, https://doi.org/10.1111/j.1365-2435.2009.01600.x, 2010b.

Berzaghi, F., Wright, I. J., Kramer, K., Oddou-Muratorio, S., Bohn, F. J., Reyer, C. P. O., Sabaté, S., Sanders, T. G. M., and Hartig, F.: Towards a New Generation of Trait-Flexible Vegetation Models, Trends in Ecology & Evolution, 35, 191–205, https://doi.org/10.1016/j.tree.2019.11.006, 2020.

Bodegom, P. M. van, Douma, J. C., and Verheijen, L. M.: A fully traits-based approach to modeling global vegetation distribution, Proceedings of the National Academy of Sciences, 111, 13733–13738, https://doi.org/10.1073/pnas.1304551110, 2014.

Boisseaux et al. submitted

BONAL, D., BOSC, A., PONTON, S., GORET, J.-Y., BURBAN, B., GROSS, P., BONNEFOND, J.-M., ELBERS, J., LONGDOZ, B., EPRON, D., GUEHL, J.-M., and GRANIER, A.: Impact of severe dry season on net ecosystem exchange in the Neotropical rainforest of French Guiana, Global Change Biology, 14, 1917–1933, https://doi.org/10.1111/j.1365-2486.2008.01610.x, 2008.

743   Bonan, G. B.: Forests and Climate Change: Forcings, Feedbacks, and the Climate Benefits of Forests, Science, 320, 1444–

744   1449, https://doi.org/10.1126/science.1155121, 2008.

745   Bugmann, H.: Climatic Change, 51, 259–305, https://doi.org/10.1023/a:1012525626267, 2001.

746   Buuren, S. van and Groothuis-Oudshoorn, K.: mice: Multivariate Imputation by Chained Equations inR, Journal of

747   Statistical Software, 45, https://doi.org/10.18637/jss.v045.i03, 2011.

748   Chave, J., Andalo, C., Brown, S., Cairns, M. A., Chambers, J. Q., Eamus, D., Fölster, H., Fromard, F., Higuchi, N., Kira,

749   T., Lescure, J.-P., Nelson, B. W., Ogawa, H., Puig, H., Riéra, B., and Yamakura, T.: Tree allometry and improved

750   estimation of carbon stocks and balance in tropical forests, Oecologia, 145, 87–99, https://doi.org/10.1007/s00442-005-

751   0100-x, 2005.

752   Chave, J., Navarrete, D., Almeida, S., Álvarez, E., Aragão, L. E. O. C., Bonal, D., Châtelet, P., Silva-Espejo, J. E., Goret,

753   J.-Y., Hildebrand, P. von, Jiménez, E., Patiño, S., Peñuela, M. C., Phillips, O. L., Stevenson, P., and Malhi, Y.: Regional

754   and seasonal patterns of litterfall in tropical South America, Biogeosciences, 7, 43–55, https://doi.org/10.5194/bg-7-43-

755   2010, 2010.

756   Chen, X., Maignan, F., Viovy, N., Bastos, A., Goll, D., Wu, J., Liu, L., Yue, C., Peng, S., Yuan, W., da Conceição, A. C.,

757   O'Sullivan, M., and Ciais, P.: Novel Representation of Leaf Phenology Improves Simulation of Amazonian Evergreen

758   Forest Photosynthesis in a Land Surface Model, Journal of Advances in Modeling Earth Systems, 12,

759   https://doi.org/10.1029/2018ms001565, 2020.

760   Chen, X., Huang, Y., Nie, C., Zhang, S., Wang, G., Chen, S., and Chen, Z.: A long-term reconstructed TROPOMI solar-

761   induced fluorescence dataset using machine learning algorithms, Scientific Data, 9, https://doi.org/10.1038/s41597-022-

762   01520-1, 2022.

763   Cuartas, L. A., Tomasella, J., Nobre, A. D., Hodnett, M. G., Waterloo, M. J., and Múnera, J. C.: Interception water-

764   partitioning dynamics for a pristine rainforest in Central Amazonia: Marked differences between normal and dry years,

765   Agricultural and Forest Meteorology, 145, 69–83, https://doi.org/10.1016/j.agrformet.2007.04.008, 2007.

766   Cui, W. and Chui, T. F. M.: Temporal and spatial variations of energy balance closure across FLUXNET research sites,

767   Agricultural and Forest Meteorology, 271, 12–21, https://doi.org/10.1016/j.agrformet.2019.02.026, 2019.

768   Cusack, D. F., Christoffersen, B., Smith-Martin, C. M., Andersen, K. M., Cordeiro, A. L., Fleischer, K., Wright, S. J.,

769   Guerrero-Ramírez, N. R., Lugli, L. F., McCulloch, L. A., Sanchez-Julia, M., Batterman, S. A., Dallstream, C., Fortunel,

770   C., Toro, L., Fuchslueger, L., Wong, M. Y., Yaffar, D., Fisher, J. B., Arnaud, M., Dietterich, L. H., Addo-Danso, S. D.,

771   Valverde-Barrantes, O. J., Weemstra, M., Ng, J. C., and Norby, R. J.: Toward a coordinated understanding of hydro-

772   biogeochemical root functions in tropical forests for application in vegetation models, New Phytologist, 242, 351–371,

773   https://doi.org/10.1111/nph.19561, 2024.

774   De Frenne, P., Zellweger, F., Rodríguez-Sánchez, F., Scheffers, B. R., Hylander, K., Luoto, M., Vellend, M., Verheyen,

775   K., and Lenoir, J.: Global buffering of temperatures under forest canopies, Nature Ecology & Evolution, 3, 744–749,

776   https://doi.org/10.1038/s41559-019-0842-1, 2019.

777   De Kauwe, M. G., Medlyn, B. E., Knauer, J., and Williams, C. A.: Ideas and perspectives: how coupled is the vegetation

778   to the boundary layer?, Biogeosciences, 14, 4435–4453, https://doi.org/10.5194/bg-14-4435-2017, 2017.

779   Diao, H., Cernusak, L. A., Saurer, M., Gessler, A., Siegwolf, R. T. W., and Lehmann, M. M.: Uncoupling of stomatal

780   conductance and photosynthesis at high temperatures: mechanistic insights from online stable isotope techniques, New

781   Phytologist, 241, 2366–2378, https://doi.org/10.1111/nph.19558, 2024.

782   Díaz-Yáñez, O., Käber, Y., Anders, T., Bohn, F., Braziunas, K. H., Brůna, J., Fischer, R., Fischer, S. M., Hetzer, J., Hickler,

783   T., Hochauer, C., Lexer, M. J., Lischke, H., Mairota, P., Merganič, J., Merganičová, K., Mette, T., Mina, M., Morin, X.,

784   Nieberg, M., Rammer, W., Reyer, C. P. O., Scheiter, S., Scherrer, D., and Bugmann, H.: Tree regeneration in models of

785   forest dynamics: A key priority for further research, Ecosphere, 15, https://doi.org/10.1002/ecs2.4807, 2024.

786   Dormann, C. F., Schymanski, S. J., Cabral, J., Chuine, I., Graham, C., Hartig, F., Kearney, M., Morin, X., Römermann, C.,

787   Schröder, B., and Singer, A.: Correlation and process in species distribution models: bridging a dichotomy, Journal of

788   Biogeography, 39, 2119–2131, https://doi.org/10.1111/j.1365-2699.2011.02659.x, 2012.

789   dos-Santos, M. N., Keller, M. M., and Morton, D. C.: LiDAR Surveys over Selected Forest Research Sites, Brazilian

790   Amazon, 2008-2018, https://doi.org/10.3334/ORNLDAAC/1644, 2019.

791   Doughty, C. E. and Goulden, M. L.: Seasonal patterns of tropical forest leaf area index and CO2 exchange, Journal of

792   Geophysical Research: Biogeosciences, 113, https://doi.org/10.1029/2007jg000590, 2008.

793   Duursma, R. A., Blackman, C. J., Lopéz, R., Martin-StPaul, N. K., Cochard, H., and Medlyn, B. E.: On the minimum leaf

794   conductance: its role in models of plant water use, and ecological and environmental controls, New Phytologist, 221, 693–

795   705, https://doi.org/10.1111/nph.15395, 2018.

796   Estes, L., Elsen, P. R., Treuer, T., Ahmed, L., Caylor, K., Chang, J., Choi, J. J., and Ellis, E. C.: The spatial and temporal

797   domains of modern ecology, Nature Ecology & Evolution, 2, 819–826, https://doi.org/10.1038/s41559-018-0524-4, 2018.

798   Evans, M. R.: Modelling ecological systems in a changing world, Philosophical Transactions of the Royal Society B:

799   Biological Sciences, 367, 181–190, https://doi.org/10.1098/rstb.2011.0172, 2012.

800   Farquhar, G. D., Caemmerer, S. von, and Berry, J. A.: A biochemical model of photosynthetic CO2 assimilation in leaves

801   of C3 species, Planta, 149, 78–90, https://doi.org/10.1007/bf00386231, 1980.

802   Fischer, F. J., Maréchaux, I., and Chave, J.: Improving plant allometry by fusing forest models and remote sensing, New

803   Phytologist, 223, 1159–1165, https://doi.org/10.1111/nph.15810, 2019.

804   Fischer, F. J., Jackson, T., Vincent, G., and Jucker, T.: Robust characterisation of forest structure from airborne laser

805   scanningA systematic assessment and sample workflow for ecologists, Methods in Ecology and Evolution,

806   https://doi.org/10.1111/2041-210x.14416, 2024.

807   Fischer, R., Bohn, F., Dantas de Paula, M., Dislich, C., Groeneveld, J., Gutiérrez, A. G., Kazmierczak, M., Knapp, N.,

808   Lehmann, S., Paulick, S., Pütz, S., Rödig, E., Taubert, F., Köhler, P., and Huth, A.: Lessons learned from applying a forest

809   gap model to understand ecosystem and carbon dynamics of complex tropical forests, Ecological Modelling, 326, 124–

810   133, https://doi.org/10.1016/j.ecolmodel.2015.11.018, 2016.

811 Fisher, J. B., Huntzinger, D. N., Schwalm, C. R., and Sitch, S.: Modeling the Terrestrial Biosphere, Annual Review of
812 Environment and Resources, 39, 91–123, https://doi.org/10.1146/annurev-environ-012913-093456, 2014.

813 Fisher, R. A., Muszala, S., Verteinstein, M., Lawrence, P., Xu, C., McDowell, N. G., Knox, R. G., Koven, C., Holm, J.,
814 Rogers, B. M., Spessa, A., Lawrence, D., and Bonan, G.: Taking off the training wheels: the properties of a dynamic
815 vegetation model without climate envelopes, CLM4.5(ED), Geoscientific Model Development, 8, 3593–3619,
816 https://doi.org/10.5194/gmd-8-3593-2015, 2015.

817 Fisher, R. A., Koven, C. D., Anderegg, W. R. L., Christoffersen, B. O., Dietze, M. C., Farrior, C. E., Holm, J. A., Hurtt, G.
818 C., Knox, R. G., Lawrence, P. J., Lichstein, J. W., Longo, M., Matheny, A. M., Medvigy, D., Muller-Landau, H. C., Powell,
819 T. L., Serbin, S. P., Sato, H., Shuman, J. K., Smith, B., Trugman, A. T., Viskari, T., Verbeeck, H., Weng, E., Xu, C., Xu,
820 X., Zhang, T., and Moorcroft, P. R.: Vegetation demographics in Earth System Models: A review of progress and priorities,
821 Global Change Biology, 24, 35–54, https://doi.org/10.1111/gcb.13910, 2017.

822 Fortunel, C., Stahl, C., Heuret, P., Nicolini, E., and Baraloto, C.: Disentangling the effects of environment and ontogeny
823 on tree functional dimensions for congeneric species in tropical forests, New Phytologist, 226, 385–395,
824 https://doi.org/10.1111/nph.16393, 2020.

825 Franklin, O., Harrison, S. P., Dewar, R., Farrior, C. E., Brännström, Å., Dieckmann, U., Pietsch, S., Falster, D., Cramer,
826 W., Loreau, M., Wang, H., Mäkelä, A., Rebel, K. T., Meron, E., Schymanski, S. J., Rovenskaya, E., Stocker, B. D., Zaehle,
827 S., Manzoni, S., Oijen, M. van, Wright, I. J., Ciais, P., Bodegom, P. M. van, Peñuelas, J., Hofhansl, F., Terrer, C.,
828 Soudzilovskaia, N. A., Midgley, G., and Prentice, I. C.: Organizing principles for vegetation dynamics, Nature Plants, 6,
829 444–453, https://doi.org/10.1038/s41477-020-0655-x, 2020.

830 Fu, R., Yin, L., Li, W., Arias, P. A., Dickinson, R. E., Huang, L., Chakraborty, S., Fernandes, K., Liebmann, B., Fisher,
831 R., and Myneni, R. B.: Increased dry-season length over southern Amazonia in recent decades and its implication for future
832 climate projection, Proceedings of the National Academy of Sciences, 110, 18110–18115,
833 https://doi.org/10.1073/pnas.1302584110, 2013.

834 Gao, Z., Liu, H., Missik, J. E. C., Yao, J., Huang, M., Chen, X., Arntzen, E., and Mcfarland, D. P.: Mechanistic links
835 between underestimated CO_2 fluxes and non-closure of the surface energy balance in a semi-arid sagebrush ecosystem,
836 Environmental Research Letters, 14, 044016, https://doi.org/10.1088/1748-9326/ab082d, 2019.

837 GONCALVES, F. G., TREUHAFT, R. N., DOS SANTOS, J. R., GRACA, P., ALMEIDA, A., and LAW, B. E.: Tree
838 Inventory and Biometry Measurements, Tapajos National Forest, Para, Brazil, 2010,
839 https://doi.org/10.3334/ORNLDAAC/1552, 2018.

840 Gourlet-Fleury, S., Guehl, J. M. J. M., & Laroussinie, O. (2004). *Ecology and management of a neotropical rainforest.*
841 *Lessons drawn from Paracou, a long-term experimental research site in French Guiana* (pp. 350-p). Elsevier.

842 Guan, K., Pan, M., Li, H., Wolf, A., Wu, J., Medvigy, D., Caylor, K. K., Sheffield, J., Wood, E. F., Malhi, Y., Liang, M.,
843 Kimball, J. S., Saleska, Scott R., Berry, J., Joiner, J., and Lyapustin, A. I.: Photosynthetic seasonality of global tropical
844 forests constrained by hydroclimate, Nature Geoscience, 8, 284–289, https://doi.org/10.1038/ngeo2382, 2015.

845 Guillemot, J., Martin-StPaul, N. K., Bulascoschi, L., Poorter, L., Morin, X., Pinho, B. X., Maire, G. le, R. L. Bittencourt,
846 P., Oliveira, R. S., Bongers, F., Brouwer, R., Pereira, L., Gonzalez Melo, G. A., Boonman, C. C. F., Brown, K. A.,
847 Cerabolini, B. E. L., Niinemets, Ü., Onoda, Y., Schneider, J. V., Sheremetiev, S., and Brancalion, P. H. S.: Small and slow
848 is safe: On the drought tolerance of tropical tree species, Global Change Biology, 28, 2622–2638,
849 https://doi.org/10.1111/gcb.16082, 2022.

850 Hanbury-Brown, A. R., Ward, R. E., and Kueppers, L. M.: Forest regeneration within Earth system models: current process
851 representations and ways forward, New Phytologist, 235, 20–40, https://doi.org/10.1111/nph.18131, 2022.

852 Harper, A., Baker, I. T., Denning, A. S., Randall, D. A., Dazlich, D., and Branson, M.: Impact of Evapotranspiration on
853 Dry Season Climate in the Amazon Forest*, Journal of Climate, 27, 574–591, https://doi.org/10.1175/jcli-d-13-00074.1,
854 2014.

855 Holthuijzen, A. M. A. and Boerboom, J. H. A.: The cecropia seedbank in the surinam lowland rain forest, Biotropica, 14,
856 62, https://doi.org/10.2307/2387761, 1982.

857 Hubau, W., Lewis, S. L., Phillips, O. L., Affum-Baffoe, K., Beeckman, H., Cuní-Sanchez, A., Daniels, A. K., Ewango, C.
858 E. N., Fauset, S., Mukinzi, J. M., Sheil, D., Sonké, B., Sullivan, M. J. P., Sunderland, T. C. H., Taedoumg, H., Thomas, S.
859 C., White, L. J. T., Abernethy, K. A., Adu-Bredu, S., Amani, C. A., Baker, T. R., Banin, L. F., Baya, F., Begne, S. K.,
860 Bennett, A. C., Benedet, F., Bitariho, R., Bocko, Y. E., Boeckx, P., Boundja, P., Brienen, R. J. W., Brncic, T., Chezeaux,
861 E., Chuyong, G. B., Clark, C. J., Collins, M., Comiskey, J. A., Coomes, D. A., Dargie, G. C., Haulleville, T. de, Kamdem,
862 M. N. D., Doucet, J.-L., Esquivel-Muelbert, A., Feldpausch, T. R., Fofanah, A., Foli, E. G., Gilpin, M., Gloor, E.,
863 Gonmadje, C., Gourlet-Fleury, S., Hall, J. S., Hamilton, A. C., Harris, D. J., Hart, T. B., Hockemba, M. B. N., Hladik, A.,
864 Ifo, S. A., Jeffery, K. J., Jucker, T., Yakusu, E. K., Kearsley, E., Kenfack, D., Koch, A., Leal, M. E., Levesley, A., Lindsell,
865 J. A., Lisingo, J., Lopez-Gonzalez, G., Lovett, J. C., Makana, J.-R., Malhi, Y., Marshall, A. R., Martin, J., Martin, E. H.,
866 Mbayu, F. M., Medjibe, V. P., Mihindou, V., Mitchard, E. T. A., Moore, S., Munishi, P. K. T., Bengone, N. N., Ojo, L.,
867 Ondo, F. E., Peh, K. S.-H., Pickavance, G. C., Poulsen, A. D., Poulsen, J. R., Qie, L., Reitsma, J., Rovero, F., Swaine, M.
868 D., Talbot, J., Taplin, J., Taylor, D. M., Thomas, D. W., Toirambe, B., Mukendi, J. T., Tuagben, D., Umunay, P. M., et al.:
869 Asynchronous carbon sink saturation in African and Amazonian tropical forests, Nature, 579, 80–87,
870 https://doi.org/10.1038/s41586-020-2035-0, 2020.

871 Huntingford, C., Atkin, O. K., Martinez-de la Torre, A., Mercado, L. M., Heskel, M. A., Harper, A. B., Bloomfield, K. J.,
872 O'Sullivan, O. S., Reich, P. B., Wythers, K. R., Butler, E. E., Chen, M., Griffin, K. L., Meir, P., Tjoelker, M. G., Turnbull,
873 M. H., Sitch, S., Wiltshire, A., and Malhi, Y.: Implications of improved representations of plant respiration in a changing
874 climate, Nature Communications, 8, https://doi.org/10.1038/s41467-017-01774-z, 2017.

875 Jaouen, G.: Paracou forest permanent plots details, https://doi.org/10.18167/DVN1/8G8AHY, 2022.

876 Joetzjer, E., Maignan, F., Chave, J., Goll, D., Poulter, B., Barichivich, J., Maréchaux, I., Luyssaert, S., Guimberteau, M.,
877 Naudts, K., Bonal, D., and Ciais, P.: Effect of tree demography and flexible root water uptake for modeling the carbon and
878 water cycles of Amazonia, Ecological Modelling, 469, 109969, https://doi.org/10.1016/j.ecolmodel.2022.109969, 2022.

879   Jucker, T., Fischer, F. J., Chave, J., Coomes, D. A., Caspersen, J., Ali, A., Loubota Panzou, G. J., Feldpausch, T. R., Falster,

880   D., Usoltsev, V. A., Adu-Bredu, S., Alves, L. F., Aminpour, M., Angoboy, I. B., Anten, N. P. R., Antin, C., Askari, Y.,

881   Muñoz, R., Ayyappan, N., Balvanera, P., Banin, L., Barbier, N., Battles, J. J., Beeckman, H., Bocko, Y. E., Bond-Lamberty,

882   B., Bongers, F., Bowers, S., Brade, T., Breugel, M. van, Chantrain, A., Chaudhary, R., Dai, J., Dalponte, M., Dimobe, K.,

883   Domec, J.-C., Doucet, J.-L., Duursma, R. A., Enríquez, M., Ewijk, K. Y. van, Farfán-Rios, W., Fayolle, A., Forni, E.,

884   Forrester, D. I., Gilani, H., Godlee, J. L., Gourlet-Fleury, S., Haeni, M., Hall, J. S., He, J.-K., Hemp, A., Hernández-

885   Stefanoni, J. L., Higgins, S. I., Holdaway, R. J., Hussain, K., Hutley, L. B., Ichie, T., Iida, Y., Jiang, H., Joshi, P. R., Kaboli,

886   H., Larsary, M. K., Kenzo, T., Kloeppel, B. D., Kohyama, T., Kunwar, S., Kuyah, S., Kvasnica, J., Lin, S., Lines, E. R.,

887   Liu, H., Lorimer, C., Loumeto, J.-J., Malhi, Y., Marshall, P. L., Mattsson, E., Matula, R., Meave, J. A., Mensah, S., Mi,

888   X., Momo, S., Moncrieff, G. R., Mora, F., Nissanka, S. P., O'Hara, K. L., Pearce, S., Pelissier, R., Peri, P. L., Ploton, P.,

889   Poorter, L., Pour, M. J., Pourbabaei, H., Dupuy-Rada, J. M., Ribeiro, S. C., Ryan, C., Sanaei, A., Sanger, J., Schlund, M.,

890   Sellan, G., et al.: Tallo: A global tree allometry and crown architecture database, Global Change Biology, 28, 5254–5268,

891   https://doi.org/10.1111/gcb.16302, 2022.

892   Kattge, J., Bönisch, G., and al., et: TRY plant trait database – enhanced coverage and open access, Global Change Biology,

893   26, 119–188, https://doi.org/10.1111/gcb.14904, 2020.

894   Kikuzawa, K.: A Cost-Benefit Analysis of Leaf Habit and Leaf Longevity of Trees and Their Geographical Pattern, The

895   American Naturalist, 138, 1250–1263, https://doi.org/10.1086/285281, 1991.

896   Knapp, N., Fischer, R., and Huth, A.: Linking lidar and forest modeling to assess biomass estimation across scales and

897   disturbance states, Remote Sensing of Environment, 205, 199–209, https://doi.org/10.1016/j.rse.2017.11.018, 2018.

898   Koch, A., Hubau, W., and Lewis, S. L.: Earth System Models Are Not Capturing Present-Day Tropical Forest Carbon

899   Dynamics, Earth's Future, 9, https://doi.org/10.1029/2020ef001874, 2021.

900   Köster, J. and Rahmann, S.: Snakemakea scalable bioinformatics workflow engine, Bioinformatics, 28, 2520–2522,

901   https://doi.org/10.1093/bioinformatics/bts480, 2012.

902   Kunert, N., Aparecido, L. M. T., Wolff, S., Higuchi, N., Santos, J. dos, Araujo, A. C. de, and Trumbore, S.: A revised

903   hydrological model for the Central Amazon: The importance of emergent canopy trees in the forest water budget,

904   Agricultural and Forest Meteorology, 239, 47–57, https://doi.org/10.1016/j.agrformet.2017.03.002, 2017.

905   Kurtzer, G. M., Sochat, V., and Bauer, M. W.: Singularity: Scientific containers for mobility of compute, PLOS ONE, 12,

906   e0177459, https://doi.org/10.1371/journal.pone.0177459, 2017.

907   Lamour, J., Davidson, K. J., Ely, K. S., Le Moguédec, G., Leakey, A. D. B., Li, Q., Serbin, S. P., and Rogers, A.: An

908   improved representation of the relationship between photosynthesis and stomatal conductance leads to more stable

909   estimation of conductance parameters and improves the goodness-of-fit across diverse data sets, Global Change Biology,

910   28, 3537–3556, https://doi.org/10.1111/gcb.16103, 2022.

911   Lapola, D. M., Pinho, P., Barlow, J., Aragão, L. E. O. C., Berenguer, E., Carmenta, R., Liddy, H. M., Seixas, H., Silva, C.

912   V. J., Silva-Junior, C. H. L., Alencar, A. A. C., Anderson, L. O., Armenteras, D., Brovkin, V., Calders, K., Chambers, J.,

913   Chini, L., Costa, M. H., Faria, B. L., Fearnside, P. M., Ferreira, J., Gatti, L., Gutierrez-Velez, V. H., Han, Z., Hibbard, K.,

914   Koven, C., Lawrence, P., Pongratz, J., Portela, B. T. T., Rounsevell, M., Ruane, A. C., Schaldach, R., Silva, S. S. da,
915   Randow, C. von, and Walker, W. S.: The drivers and impacts of Amazon forest degradation, Science, 379,
916   https://doi.org/10.1126/science.abp8622, 2023.

917   Lawrence, D. and Vandecar, K.: Effects of tropical deforestation on climate and agriculture, Nature Climate Change, 5,
918   27–36, https://doi.org/10.1038/nclimate2430, 2014.

919   Long, S. P., Postl, W. F., and Bolher-Nordenkampf, H. R.: Quantum yields for uptake of carbon dioxide in C3 vascular
920   plants of contrasting habitats and taxonomic groupings, Planta, 189, https://doi.org/10.1007/bf00195081, 1993.

921   Longo, M., Knox, R. G., Levine, N. M., Alves, L. F., Bonal, D., Camargo, P. B., Fitzjarrald, D. R., Hayek, M. N., Restrepo-
922   Coupe, N., Saleska, S. R., Silva, R. da, Stark, S. C., Tapajós, R. P., Wiedemann, K. T., Zhang, K., Wofsy, S. C., and
923   Moorcroft, P. R.: Ecosystem heterogeneity and diversity mitigate Amazon forest resilience to frequent extreme droughts,
924   New Phytologist, 219, 914–931, https://doi.org/10.1111/nph.15185, 2018.

925   Longo, M., Knox, R. G., Medvigy, D. M., Levine, N. M., Dietze, M. C., Kim, Y., Swann, A. L. S., Zhang, K., Rollinson,
926   C. R., Bras, R. L., Wofsy, S. C., and Moorcroft, P. R.: The biophysics, ecology, and biogeochemistry of functionally
927   diverse, vertically and horizontally heterogeneous ecosystems: the Ecosystem Demography model, version 2.2 Part 1:
928   Model description, Geoscientific Model Development, 12, 4309–4346, https://doi.org/10.5194/gmd-12-4309-2019, 2019a.

929   Longo, M., Knox, R. G., Levine, N. M., Swann, A. L. S., Medvigy, D. M., Dietze, M. C., Kim, Y., Zhang, K., Bonal, D.,
930   Burban, B., Camargo, P. B., Hayek, M. N., Saleska, S. R., Silva, R. da, Bras, R. L., Wofsy, S. C., and Moorcroft, P. R.:
931   The biophysics, ecology, and biogeochemistry of functionally diverse, vertically and horizontally heterogeneous
932   ecosystems: the Ecosystem Demography model, version 2.2 Part 2: Model evaluation for tropical South America,
933   Geoscientific Model Development, 12, 4347–4374, https://doi.org/10.5194/gmd-12-4347-2019, 2019b.

934   Malhi, Y., Doughty, C., and Galbraith, D.: The allocation of ecosystem net primary productivity in tropical forests,
935   Philosophical   Transactions   of   the   Royal   Society   B: Biological   Sciences,   366,   3225–3245,
936   https://doi.org/10.1098/rstb.2011.0062, 2011.

937   Maréchaux, I., Bartlett, M. K., Sack, L., Baraloto, C., Engel, J., Joetzjer, E., and Chave, J.: Drought tolerance as predicted
938   by leaf water potential at turgor loss point varies strongly across species within an Amazonian forest, Functional Ecology,
939   29, 1268–1277, https://doi.org/10.1111/1365-2435.12452, 2015.

940   Maréchaux, I., Saint-André, L., Bartlett, M. K., Sack, L., and Chave, J.: Leaf drought tolerance cannot be inferred from
941   classic leaf traits in a tropical rainforest, Journal of Ecology, 108, 1030–1045, https://doi.org/10.1111/1365-2745.13321,
942   2019.

943   Maréchaux, I., Langerwisch, F., Huth, A., Bugmann, H., Morin, X., Reyer, C. P. O., Seidl, R., Collalti, A., Dantas de Paula,
944   M., Fischer, R., Gutsch, M., Lexer, M. J., Lischke, H., Rammig, A., Rödig, E., Sakschewski, B., Taubert, F., Thonicke, K.,
945   Vacchiano, G., and Bohn, F. J.: Tackling unresolved questions in forest ecology: The past and future role of simulation
946   models, Ecology and Evolution, 11, 3746–3770, https://doi.org/10.1002/ece3.7391, 2021.

947   Marrs, J. K., Reblin, J. S., Logan, B. A., Allen, D. W., Reinmann, A. B., Bombard, D. M., Tabachnik, D., and Hutyra, L.
948   R.: Solar-Induced Fluorescence Does Not Track Photosynthetic Carbon Assimilation Following Induced Stomatal Closure,
949   Geophysical Research Letters, 47, https://doi.org/10.1029/2020gl087956, 2020.

950   McMahon, S. M., Harrison, S. P., Armbruster, W. S., Bartlein, P. J., Beale, C. M., Edwards, M. E., Kattge, J., Midgley, G.,
951   Morin, X., and Prentice, I. C.: Improving assessment and modelling of climate change impacts on global terrestrial
952   biodiversity, Trends in Ecology & Evolution, 26, 249–259, https://doi.org/10.1016/j.tree.2011.02.012, 2011.

953   Medlyn, B. E., Robinson, A. P., Clement, R., and McMurtrie, R. E.: On the validation of models of forest CO2 exchange
954   using eddy covariance data: some perils and pitfalls, Tree Physiology, 25, 839–857,
955   https://doi.org/10.1093/treephys/25.7.839, 2005.

956   Medlyn, B. E., Duursma, R. A., De Kauwe, M. G., and Prentice, I. C.: The optimal stomatal response to atmospheric CO2
957   concentration: Alternative solutions, alternative interpretations, Agricultural and Forest Meteorology, 182-183, 200–203,
958   https://doi.org/10.1016/j.agrformet.2013.04.019, 2013.

959   Meir, P., Grace, J., and Miranda, A. C.: Photographic method to measure the vertical distribution of leaf area density in
960   forests, Agricultural and Forest Meteorology, 102, 105–111, https://doi.org/10.1016/s0168-1923(00)00122-2, 2000.

961   Merganičová, K., Merganič, J., Lehtonen, A., Vacchiano, G., Sever, M. Z. O., Augustynczik, A. L. D., Grote, R., Kyselová,
962   I, Mäkelä, A., Yousefpour, R., Krejza, J., Collalti, A., and Reyer, C. P. O.: Forest carbon allocation modelling under
963   climate change, Tree Physiology, 39, 1937–1960, https://doi.org/10.1093/treephys/tpz105, 2019.

964   Meunier, F., Verbruggen, W., Verbeeck, H., and Peaucelle, M.: Low sensitivity of three terrestrial biosphere models to soil
965   texture over the South American tropics, Geoscientific Model Development, 15, 7573–7591, https://doi.org/10.5194/gmd-
966   15-7573-2022, 2022.

967   Mokany, K., Ferrier, S., Connolly, S. R., Dunstan, P. K., Fulton, E. A., Harfoot, M. B., Harwood, T. D., Richardson, A. J.,
968   Roxburgh, S. H., Scharlemann, J. P. W., Tittensor, D. P., Westcott, D. A., and Wintle, B. A.: Integrating modelling of
969   biodiversity composition and ecosystem function, Oikos, 125, 10–19, https://doi.org/10.1111/oik.02792, 2015.

970   Montgomery, R. A. and Chazdon, R. L.: FOREST STRUCTURE, CANOPY ARCHITECTURE, AND LIGHT
971   TRANSMITTANCE IN TROPICAL WET FORESTS, Ecology, 82, 2707–2718, https://doi.org/10.1890/0012-
972   9658(2001)082[2707:fscaal]2.0.co;2, 2001.

973   Moorcroft, P. R., Hurtt, G. C., and Pacala, S. W.: A METHOD FOR SCALING VEGETATION DYNAMICS: THE
974   ECOSYSTEM DEMOGRAPHY MODEL (ED), Ecological Monographs, 71, 557–586, https://doi.org/10.1890/0012-
975   9615(2001)071[0557:amfsvd]2.0.co;2, 2001.

976   Muller-Landau, H. C.: The tolerancefecundity trade-off and the maintenance of diversity in seed size, Proceedings of the
977   National Academy of Sciences, 107, 4242–4247, https://doi.org/10.1073/pnas.0911637107, 2010.

978   Muñoz-Sabater, J., Dutra, E., Agustí-Panareda, A., Albergel, C., Arduini, G., Balsamo, G., Boussetta, S., Choulga, M.,
979   Harrigan, S., Hersbach, H., Martens, B., Miralles, D. G., Piles, M., Rodríguez-Fernández, N. J., Zsoter, E., Buontempo, C.,
980   and Thépaut, J.-N.: ERA5-Land: a state-of-the-art global reanalysis dataset for land applications, Earth System Science
981   Data, 13, 4349–4383, https://doi.org/10.5194/essd-13-4349-2021, 2021.

982   Nemetschek, D., Derroire, G., Marcon, E., Aubry-Kientz, M., Auer, J., Badouard, V., Baraloto, C., Bauman, D., Le Blaye,
983   Q., Boisseaux, M., Bonal, D., Coste, S., Dardevet, E., Heuret, P., Hietz, P., Levionnois, S., Maréchaux, I., McMahon, S.
984   M., Stahl, C., Vleminckx, J., Wanek, W., Ziegler, C., and Fortunel, C.: Climate anomalies and neighbourhood crowding
985   interact in shaping tree growth in old-growth and selectively logged tropical forests, Journal of Ecology,
986   https://doi.org/10.1111/1365-2745.14256, 2024.

987   Nepstad, D. C., Moutinho, P., Dias-Filho, M. B., Davidson, E., Cardinot, G., Markewitz, D., Figueiredo, R., Vianna, N.,
988   Chambers, J., Ray, D., Guerreiros, J. B., Lefebvre, P., Sternberg, L., Moreira, M., Barros, L., Ishida, F. Y., Tohlver, I.,
989   Belk, E., Kalif, K., and Schwalbe, K.: The effects of partial throughfall exclusion on canopy processes, aboveground
990   production, and biogeochemistry of an Amazon forest, Journal of Geophysical Research: Atmospheres, 107,
991   https://doi.org/10.1029/2001jd000360, 2002.

992   Nunes, M. H., Camargo, J. L. C., Vincent, G., Calders, K., Oliveira, R. S., Huete, A., Mendes de Moura, Y., Nelson, B.,
993   Smith, M. N., Stark, S. C., and Maeda, E. E.: Forest fragmentation impacts the seasonality of Amazonian evergreen
994   canopies, Nature Communications, 13, https://doi.org/10.1038/s41467-022-28490-7, 2022.

995   Paschalis, A., De Kauwe, M. G., Sabot, M., and Fatichi, S.: When do plant hydraulics matter in terrestrial biosphere
996   modelling?, Global Change Biology, 30, https://doi.org/10.1111/gcb.17022, 2023.

997   Pastorello, Gilberto, Trotta, Carlo, Canfora, Eleonora, Chu, Housen, Christianson, Danielle, Cheah, You-Wei, Poindexter,
998   Cristina, Chen, Jiquan, Elbashandy, Abdelrahman, Humphrey, Marty, Isaac, Peter, Polidori, Diego, Ribeca, Alessio, van
999   Ingen, Catharine, Zhang, Leiming, Amiro, Brian, Ammann, Christof, Arain, M Altaf, Ardö, Jonas, Arkebauer, Timothy,
1000   Arndt, Stefan K, Arriga, Nicola, Aubinet, Marc, Aurela, Mika, Baldocchi, Dennis, Barr, Alan, Beamesderfer, Eric,
1001   Marchesini, Luca Belelli, Bergeron, Onil, Beringer, Jason, Paul-Limoges, Eugénie, and et al: The FLUXNET2015 dataset
1002   and the ONEFlux processing pipeline for eddy covariance data, Nature Publishing Group, https://doi.org/10.5167/UZH-
1003   190509, 2020.

1004   Poorter, L., Oberbauer, S. F., and Clark, D. B.: LEAF OPTICAL PROPERTIES ALONG A VERTICAL GRADIENT IN
1005   A TROPICAL RAIN FOREST CANOPY IN COSTA RICA, American Journal of Botany, 82, 1257–1263,
1006   https://doi.org/10.1002/j.1537-2197.1995.tb12659.x, 1995.

1007   Powell, T. L., Galbraith, D. R., Christoffersen, B. O., Harper, A., Imbuzeiro, H. M. A., Rowland, L., Almeida, S., Brando,
1008   P. M., Costa, A. C. L. da, Costa, M. H., Levine, N. M., Malhi, Y., Saleska, S. R., Sotta, E., Williams, M., Meir, P., and
1009   Moorcroft, P. R.: Confronting model predictions of carbon fluxes with measurements of Amazon forests subjected to
1010   experimental drought, New Phytologist, 200, 350–365, https://doi.org/10.1111/nph.12390, 2013.

1011   Prentice, I. C., Liang, X., Medlyn, B. E., and Wang, Y.-P.: Reliable, robust and realistic: the three R's of next-generation
1012   land-surface modelling, Atmospheric Chemistry and Physics, 15, 5987–6005, https://doi.org/10.5194/acp-15-5987-2015,
1013   2015.

1014   Purves, D. and Pacala, S.: Predictive Models of Forest Dynamics, Science, 320, 1452–1453,
1015   https://doi.org/10.1126/science.1155359, 2008.

1016   Qie, L., Lewis, S. L., Sullivan, M. J. P., Lopez-Gonzalez, G., Pickavance, G. C., Sunderland, T., Ashton, P., Hubau, W.,
1017   Abu Salim, K., Aiba, S.-I., Banin, L. F., Berry, N., Brearley, F. Q., Burslem, D. F. R. P., Dančák, M., Davies, S. J.,
1018   Fredriksson, G., Hamer, K. C., Hédl, R., Kho, L. K., Kitayama, K., Krisnawati, H., Lhota, S., Malhi, Y., Maycock, C.,
1019   Metali, F., Mirmanto, E., Nagy, L., Nilus, R., Ong, R., Pendry, C. A., Poulsen, A. D., Primack, R. B., Rutishauser, E.,
1020   Samsoedin, I., Saragih, B., Sist, P., Slik, J. W. F., Sukri, R. S., Svátek, M., Tan, S., Tjoa, A., Nieuwstadt, M. van,
1021   Vernimmen, R. R. E., Yassir, I., Kidd, P. S., Fitriadi, M., Ideris, N. K. H., Serudin, R. M., Abdullah Lim, L. S., Saparudin,
1022   M. S., and Phillips, O. L.: Long-term carbon sink in Borneo's forests halted by drought and vulnerable to edge effects,
1023   Nature Communications, 8, https://doi.org/10.1038/s41467-017-01997-0, 2017.

1024   Quesada, C. A., Lloyd, J., Schwarz, M., Patiño, S., Baker, T. R., Czimczik, C., Fyllas, N. M., Martinelli, L., Nardoto, G.
1025   B., Schmerler, J., Santos, A. J. B., Hodnett, M. G., Herrera, R., Luizão, F. J., Arneth, A., Lloyd, G., Dezzeo, N., Hilke, I.,
1026   Kuhlmann, I., Raessler, M., Brand, W. A., Geilmann, H., Moraes Filho, J. O., Carvalho, F. P., Araujo Filho, R. N., Chaves,
1027   J. E., Cruz Junior, O. F., Pimentel, T. P., and Paiva, R.: Variations in chemical and physical properties of Amazon forest
1028   soils in relation to their genesis, Biogeosciences, 7, 1515–1541, https://doi.org/10.5194/bg-7-1515-2010, 2010.

1029   Reichstein, M., Falge, E., Baldocchi, D., Papale, D., Aubinet, M., Berbigier, P., Bernhofer, C., Buchmann, N., Gilmanov,
1030   T., Granier, A., Grünwald, T., Havránková, K., Ilvesniemi, H., Janous, D., Knohl, A., Laurila, T., Lohila, A., Loustau, D.,
1031   Matteucci, G., Meyers, T., Miglietta, F., Ourcival, J.-M., Pumpanen, J., Rambal, S., Rotenberg, E., Sanz, M., Tenhunen,
1032   J., Seufert, G., Vaccari, F., Vesala, T., Yakir, D., and Valentini, R.: On the separation of net ecosystem exchange into
1033   assimilation and ecosystem respiration: review and improved algorithm, Global Change Biology, 11, 1424–1439,
1034   https://doi.org/10.1111/j.1365-2486.2005.001002.x, 2005.

1035   Restrepo-Coupe, N., Levine, N. M., Christoffersen, B. O., Albert, L. P., Wu, J., Costa, M. H., Galbraith, D., Imbuzeiro, H.,
1036   Martins, G., Araujo, A. C. da, Malhi, Y. S., Zeng, X., Moorcroft, P., and Saleska, S. R.: Do dynamic global vegetation
1037   models capture the seasonality of carbon fluxes in the Amazon basin? A data-model intercomparison, Global Change
1038   Biology, 23, 191–208, https://doi.org/10.1111/gcb.13442, 2016.

1039   Restrepo-Coupe, N., Campos, K. S., Alves, L. F., Longo, M., Wiedemann, K. T., Oliveira, R. C. de, Aragao, L. E. O. C.,
1040   Christoffersen, B. O., Camargo, P. B., Figueira, A. M. e. S., Ferreira, M. L., Oliveira, R. S., Penha, D., Prohaska, N.,
1041   Araujo, A. C. da, Daube, B. C., Wofsy, S. C., and Saleska, S. R.: Contrasting carbon cycle responses to dry (2015 El Niño)
1042   and wet (2008 La Niña) extreme events at an Amazon tropical forest, Agricultural and Forest Meteorology, 353, 110037,
1043   https://doi.org/10.1016/j.agrformet.2024.110037, 2024.

1044   RICE, A. H., HAMMOND, E. P., SALESKA, S. R., HUTYRA, L. R., PALACE, M. W., KELLER, M. M., DE
1045   CAMARGO, P. B., PORTILHO, K., MARQUES, D., and WOFSY, S. C.: LBA-ECO CD-10 Forest Litter Data for km 67
1046   Tower Site, Tapajos National Forest, https://doi.org/10.3334/ORNLDAAC/862, 2008.

1047   Ross, J.: Net radiation in plant stands, Springer Netherlands, 344–353, https://doi.org/10.1007/978-94-009-8647-3_19,
1048   1981.

1049   Rutishauser, E., Wagner, F., Herault, B., Nicolini, E.-A., and Blanc, L.: Contrasting above-ground biomass balance in a
1050   Neotropical rain forest, Journal of Vegetation Science, https://doi.org/10.1111/j.1654-1103.2010.01175.x, 2010.

1051   Sabatier, D., Grimaldi, M., Prévost, M.-F., Guillaume, J., Godron, M., Dosso, M., and Sabatier, D.: The influence of soil
1052   cover organization on the floristic and structural heterogeneity of a Guianan rain forest, Plant Ecology formerly
1053   "Vegetatio," 131, 81–108, https://doi.org/10.1023/a:1009775025850, 1997.

1054   Sabot, M., De Kauwe, M., Medlyn, B., and Pitman, A.: One stomatal model to rule them all? Evaluating competing
1055   hypotheses to regulate the exchange of carbon and water against experimental data, 2020.

1056   Sakschewski, B., Bloh, W. von, Boit, A., Rammig, A., Kattge, J., Poorter, L., Peñuelas, J., and Thonicke, K.: Leaf and
1057   stem economics spectra drive diversity of functional plant traits in a dynamic global vegetation model, Global Change
1058   Biology, 21, 2711–2725, https://doi.org/10.1111/gcb.12870, 2015.

1059   Saleska, S. R., Miller, S. D., Matross, D. M., Goulden, M. L., Wofsy, S. C., Rocha, H. R. da, Camargo, P. B. de, Crill, P.,
1060   Daube, B. C., Freitas, H. C. de, Hutyra, L., Keller, M., Kirchhoff, V., Menton, M., Munger, J. W., Pyle, E. H., Rice, A. H.,
1061   and Silva, H.: Carbon in Amazon Forests: Unexpected Seasonal Fluxes and Disturbance-Induced Losses, Science, 302,
1062   1554–1557, https://doi.org/10.1126/science.1091165, 2003.

1063   Scheiter, S., Langan, L., and Higgins, S. I.: Next-generation dynamic global vegetation models: learning from community
1064   ecology, New Phytologist, 198, 957–969, https://doi.org/10.1111/nph.12210, 2013.

1065   Schmitt, S. and Boisseaux, M.: Higher local intra- than interspecific variability in water- and carbon-related leaf traits
1066   among Neotropical tree species, Annals of Botany, 131, 801–811, https://doi.org/10.1093/aob/mcad042, 2023.

1067   Schmitt, S., Salzet, G., Fischer, F. J., Maréchaux, I., and Chave, J.: rcontroll: An R interface for the individual-based forest
1068   dynamics simulator TROLL, Methods in Ecology and Evolution, 14, 2749–2757, https://doi.org/10.1111/2041-
1069   210x.14215, 2023.

1070   Silver, W. L., Neff, J., McGroddy, M., Veldkamp, E., Keller, M., and Cosme, R.: Effects of soil texture on belowground
1071   carbon and nutrient storage in a lowland amazonian forest ecosystem, Ecosystems, 3, 193–209,
1072   https://doi.org/10.1007/s100210000019, 2000.

1073   Slot, M., Rifai, S. W., Eze, C. E., and Winter, K.: The stomatal response to vapor pressure deficit drives the apparent
1074   temperature response of photosynthesis in tropical forests, New Phytologist, https://doi.org/10.1111/nph.19806, 2024.

1075   Smith, B., Prentice, I. C., and Sykes, M. T.: Representation of vegetation dynamics in the modelling of terrestrial
1076   ecosystems: comparing two contrasting approaches within European climate space, Global Ecology and Biogeography, 10,
1077   621–637, https://doi.org/10.1046/j.1466-822x.2001.t01-1-00256.x, 2001.

1078   Smith, M. N., Stark, S. C., Taylor, T. C., Ferreira, M. L., Oliveira, E. de, Restrepo-Coupe, N., Chen, S., Woodcock, T.,
1079   Santos, D. B. dos, Alves, L. F., Figueira, M., Camargo, P. B. de, Oliveira, R. C. de, Aragão, L. E. O. C., Falk, D. A.,
1080   McMahon, S. M., Huxman, T. E., and Saleska, S. R.: Seasonal and drought-related changes in leaf area profiles depend on
1081   height and light environment in an Amazon forest, New Phytologist, 222, 1284–1297, https://doi.org/10.1111/nph.15726,
1082   2019.

1083   Thuiller, W., Albert, C., Araújo, M. B., Berry, P. M., Cabeza, M., Guisan, A., Hickler, T., Midgley, G. F., Paterson, J.,
1084   Schurr, F. M., Sykes, M. T., and Zimmermann, N. E.: Predicting global change impacts on plant species' distributions:

1085   Future challenges, Perspectives in Plant Ecology, Evolution and Systematics, 9, 137–152,
1086   https://doi.org/10.1016/j.ppees.2007.09.004, 2008.

1087   Trugman, A. T., Medvigy, D., Mankin, J. S., and Anderegg, W. R. L.: Soil Moisture Stress as a Major Driver of Carbon
1088   Cycle Uncertainty, Geophysical Research Letters, 45, 6495–6503, https://doi.org/10.1029/2018gl078131, 2018.

1089   Ukkola, A.: PLUMBER2: forcing and evaluation datasets for a model intercomparison project for land surface models
1090   v1.0, https://doi.org/10.25914/5FDB0902607E1, 2020.

1091   Van Langenhove, L., Verryckt, L. T., Bréchet, L., Courtois, E. A., Stahl, C., Hofhansl, F., Bauters, M., Sardans, J., Boeckx,
1092   P., Fransen, E., Peñuelas, J., and Janssens, I. A.: Atmospheric deposition of elements and its relevance for nutrient budgets
1093   of tropical forests, Biogeochemistry, 149, 175–193, https://doi.org/10.1007/s10533-020-00673-8, 2020.

1094   Van Langenhove, L., Depaepe, T., Verryckt, L. T., Vallicrosa, H., Fuchslueger, L., Lugli, L. F., Bréchet, L., Ogaya, R.,
1095   Llusia, J., Urbina, I., Gargallo-Garriga, A., Grau, O., Richter, A., Penuelas, J., Van Der Straeten, D., and Janssens, I. A.:
1096   Impact of Nutrient Additions on Free-Living Nitrogen Fixation in Litter and Soil of Two French-Guianese Lowland
1097   Tropical Forests, Journal of Geophysical Research: Biogeosciences, 126, https://doi.org/10.1029/2020jg006023, 2021.

1098   Villarreal, S. and Vargas, R.: Representativeness of FLUXNET Sites Across Latin America, Journal of Geophysical
1099   Research: Biogeosciences, 126, https://doi.org/10.1029/2020jg006090, 2021.

1100   Vincent, G., Antin, C., Laurans, M., Heurtebize, J., Durrieu, S., Lavalley, C., and Dauzat, J.: Mapping plant area index of
1101   tropical evergreen forest by airborne laser scanning. A cross-validation study using LAI2200 optical sensor, Remote
1102   Sensing of Environment, 198, 254–266, https://doi.org/10.1016/j.rse.2017.05.034, 2017.

1103   VINCENT, G., PIMONT, F., and VERLEY, P.: Various PAD/LAD estimators implemented in AMAPVox 1.8,
1104   https://doi.org/10.23708/1AJNMP, 2021.

1105   Vincent, G., Verley, P., Brede, B., Delaitre, G., Maurent, E., Ball, J., Clocher, I., and Barbier, N.: Multi-sensor airborne
1106   lidar requires intercalibration for consistent estimation of light attenuation and plant area density, Remote Sensing of
1107   Environment, 286, 113442, https://doi.org/10.1016/j.rse.2022.113442, 2023.

1108   Vleminckx, J., Fortunel, C., Valverde-Barrantes, O., Timothy Paine, C. E., Engel, J., Petronelli, P., Dourdain, A. K.,
1109   Guevara, J., Béroujon, S., and Baraloto, C.: Resolving whole-plant economics from leaf, stem and root traits of 1467
1110   Amazonian tree species, Oikos, 130, 1193–1208, https://doi.org/10.1111/oik.08284, 2021.

1111   Wagner, F. H., Hérault, B., Bonal, D., Stahl, C., Anderson, L. O., Baker, T. R., Becker, G. S., Beeckman, H., Boanerges
1112   Souza, D., Botosso, P. C., Bowman, D. M. J. S., Bräuning, A., Brede, B., Brown, F. I., Camarero, J. J., Camargo, P. B.,
1113   Cardoso, F. C. G., Carvalho, F. A., Castro, W., Chagas, R. K., Chave, J., Chidumayo, E. N., Clark, D. A., Costa, F. R. C.,
1114   Couralet, C., Silva Mauricio, P. H. da, Dalitz, H., Castro, V. R. de, Freitas Milani, J. E. de, Oliveira, E. C. de, Souza Arruda,
1115   L. de, Devineau, J.-L., Drew, D. M., Dünisch, O., Durigan, G., Elifuraha, E., Fedele, M., Ferreira Fedele, L., Figueiredo
1116   Filho, A., Finger, C. A. G., Franco, A. C., Freitas Júnior, J. L., Galvão, F., Gebrekirstos, A., Gliniars, R., Graça, P. M. L.
1117   de A., Griffiths, A. D., Grogan, J., Guan, K., Homeier, J., Kanieski, M. R., Kho, L. K., Koenig, J., Kohler, S. V.,
1118   Krepkowski, J., Lemos-Filho, J. P., Lieberman, D., Lieberman, M. E., Lisi, C. S., Longhi Santos, T., López Ayala, J. L.,
1119   Maeda, E. E., Malhi, Y., Maria, V. R. B., Marques, M. C. M., Marques, R., Maza Chamba, H., Mbwambo, L., Melgaço,

1120   K. L. L., Mendivelso, H. A., Murphy, B. P., O'Brien, J. J., Oberbauer, S. F., Okada, N., Pélissier, R., Prior, L. D., Roig, F.

1121   A., Ross, M., Rossatto, D. R., Rossi, V., Rowland, L., Rutishauser, E., Santana, H., Schulze, M., Selhorst, D., Silva, W.

1122   R., Silveira, M., Spannl, S., Swaine, M. D., Toledo, J. J., Toledo, M. M., Toledo, M., Toma, T., Tomazello Filho, M.,

1123   Valdez Hernández, J. I., Verbesselt, J., Vieira, S. A., Vincent, G., Volkmer de Castilho, C., et al.: Climate seasonality limits

1124   leaf carbon assimilation and wood productivity in tropical forests, Biogeosciences, 13, 2537–2562,

1125   https://doi.org/10.5194/bg-13-2537-2016, 2016.

1126   Wu, J., Albert, L. P., Lopes, A. P., Restrepo-Coupe, N., Hayek, M., Wiedemann, K. T., Guan, K., Stark, S. C.,

1127   Christoffersen, B., Prohaska, N., Tavares, J. V., Marostica, S., Kobayashi, H., Ferreira, M. L., Campos, K. S., Silva, R. da,

1128   Brando, P. M., Dye, D. G., Huxman, T. E., Huete, A. R., Nelson, B. W., and Saleska, S. R.: Leaf development and

1129   demography explain photosynthetic seasonality in Amazon evergreen forests, Science, 351, 972–976,

1130   https://doi.org/10.1126/science.aad5068, 2016.

1131   Wu, J., Serbin, S. P., Xu, X., Albert, L. P., Chen, M., Meng, R., Saleska, S. R., and Rogers, A.: The phenology of leaf

1132   quality and its within-canopy variation is essential for accurate modeling of photosynthesis in tropical evergreen forests,

1133   Global Change Biology, 23, 4814–4827, https://doi.org/10.1111/gcb.13725, 2017.

1134   Wu, W., Sun, Y., Xiao, K., and Xin, Q.: Development of a global annual land surface phenology dataset for 19822018

1135   from the AVHRR data by implementing multiple phenology retrieving methods, International Journal of Applied Earth

1136   Observation and Geoinformation, 103, 102487, https://doi.org/10.1016/j.jag.2021.102487, 2021.

1137   Yang, X., Wu, J., Chen, X., Ciais, P., Maignan, F., Yuan, W., Piao, S., Yang, S., Gong, F., Su, Y., Dai, Y., Liu, L., Zhang,

1138   H., Bonal, D., Liu, H., Chen, G., Lu, H., Wu, S., Fan, L., Gentine, P., and Wright, S. J.: A comprehensive framework for

1139   seasonal controls of leaf abscission and productivity in evergreen broadleaved tropical and subtropical forests, The

1140   Innovation, 2, 100154, https://doi.org/10.1016/j.xinn.2021.100154, 2021.

1141   Yang, X., Chen, X., Ren, J., Yuan, W., Liu, L., Liu, J., Chen, D., Xiao, Y., Wu, S., Fan, L., Dai, X., and Su, Y.: A grid

1142   dataset of leaf age-dependent LAI seasonality product (lad-LAI) over tropical and subtropical evergreen broadleaved

1143   forests, 2023.

1144   Yao, Y., Ciais, P., Viovy, N., Joetzjer, E., and Chave, J.: How drought events during the last century have impacted biomass

1145   carbon in Amazonian rainforests, Global Change Biology, 29, 747–762, https://doi.org/10.1111/gcb.16504, 2022.

1146   Yuan, Q.: Semantic-based clustering for 3D instance segmentation in sparse radar point clouds, 2023 International

1147   Conference on Algorithms, Computing and Data Processing (ACDP), 9370, 209–216,

1148   https://doi.org/10.1109/acdp59959.2023.00041, 2023.

1149   Ziegler, C., Coste, S., Stahl, C., Delzon, S., Levionnois, S., Cazal, J., Cochard, H., Esquivel-Muelbert, A., Goret, J.-Y.,

1150   Heuret, P., Jaouen, G., Santiago, L. S., and Bonal, D.: Large hydraulic safety margins protect Neotropical canopy rainforest

1151   tree species against hydraulic failure during drought, Annals of Forest Science, 76, https://doi.org/10.1007/s13595-019-

1152   0905-0, 2019.

1153 **Appendix**

1154 **Table A1: TROLL 4.0 global parameters.**

Abbreviation	Definition	Units	Value	Nature*	Reference
c_a	Carbon free air concentration	µmol mol^{-1}	375	Constant	
P_{ress}	Atmospheric pressure	kPa	101	Constant	
k_{geom}	Light extinction coefficient, reflecting leaf geometric arrangement	unitless	0.5	Constant	Ross 1981
absorptance$_{leaves}$	leaves absorptance	unitless	0.83	Literature	Long et al., 1993; Poorter et al., 1995
θ	Curvature factor (Farquhar model parameter)	unitless	0.7	Literature	Farquhar et al., 1980
g_0	leaf minimum conductance for water vapor	mmol H$_2$0 m^{-2} s^{-1}	5	Literature	Duursma et al., 2019
$a_{T,o}$	Phenological parameter that modulates old leaf drought tolerance	unitless		Calibrated	
$b_{T,o}$	Phenological parameter that modulates the height dependence of leaf susceptibility to drought	MPa		Calibrated	
δ_o	Phenological parameter that controls the pace of old leaf shedding acceleration	unitless		Calibrated	
f_{wood}	Fraction of carbon allocated to wood	unitless	0.35	Literature	Aragão et al., 2019; Malhi et al., 2011
f_{canopy}	Fraction of carbon allocated to canopy		0.25	Literature	Aragão et al., 2019; Malhi et al., 2011
f_{gap}	Fraction of gaps in the tree crown		0.15	Literature	Fischer et al., 2019

a_{CR}	Crown radius intercept	unitless		Calibrated	
b_{CR}	Crown radius slope	unitless		Calibrated	
a_{CD}	Crown depth intercept	m	0	Literature	Chave et al., 2005
b_{CD}	Crown depth slope	unitless	0.2	Literature	Chave et al., 2005
$shape_{crown}$	Crown shape parameter		0.72	Calibrated	
N_{tot}	Intensity of the external seed rain	seeds ha^{-1}	50,000	Assumed	
n_s	Number of reproduction opportunities per mature tree	seeds tree^{-1}	10	Assumed	
m	Reference background mortality	death year^{-1}		Calibrated	
v_T	Variance of the flexion moment for treefall		0.021	Calibrated	
σ_h	Intraspecific variation in height (log scale)	m	0.19	Inferred	Baraloto et al., 2010
σ_{cr}	Intraspecific variation in crown radius (log scale)	m	0.29	Calibrated	Fischer et al., 2019
σ_{cd}	Intraspecific variation in crown depth (log scale)	m	0		
σ_{dbhmax}	Intraspecific variation in maximum diameters (log scale)	m	0.05	Inferred	Baraloto et al., 2010
$corr_{cr-h}$	Intraspecific correlation between crown radius and height		0		
σ_P	Intraspecific variation in phosphorus (log scale)	mg g^{-1}	0.24	Inferred	Baraloto et al., 2010
σ_N	Intraspecific variation in nitrogen (log scale)	mg g^{-1}	0.12	Inferred	Baraloto et al., 2010
σ_{LMA}	Intraspecific variation in leaf mass per area (log scale)	g m^{-2}	0.24	Inferred	Baraloto et al., 2010

σ_{wsg}	Intraspecific variation in wood specific gravity	g cm^{-3}	0.06	Inferred	Baraloto et al., 2010
σ_{LA}	Intraspecific variation in leaf area (log scale)	cm^2	0.48	Inferred	Schmitt and Boisseaux 2023
σ_{tlp}	Intraspecific variation in turgor loss point (log scale)	MPa	0.10	Inferred	Schmitt and Boisseaux 2023
$corr_{N-P}$	Intraspecific correlation between nitrogen and phosphorous		0.65	Inferred	Baraloto et al., 2010
$corr_{N-LMA}$	Intraspecific correlation between nitrogen and leaf mass per area		-0.43	Inferred	Baraloto et al., 2010
$corr_{P-LMA}$	Intraspecific correlation between phosphorus and leaf mass per area		-0.39	Inferred	Baraloto et al., 2010

1155 *Assumed is a value that is supposed; Calibrated is a value that was previously calibrated; Constant is a fundamental physic constant;
1156 Literature is a value prescribed from the literature.

1157

1158 **Table A2: Evaluation of forest structure, composition and fluxes explored at Paracou and Tapajos. Evaluations include the goodness-**
1159 **of-fit R^2 from the linear regression with a null intercept, the Pearson's r correlation coefficient CC, the root mean square error of**
1160 **prediction RMSEP, the standard deviation of the error of prediction SD.**

| Site	Variable	Unit	Observations	Temporal resolution	R^2	CC	RMSEP	SD
Paracou	height	%	Plane	single	0.93	0.95	0.76	0.76
Tapajos	height	%	Plane	single	0.94	0.94	0.56	0.55
Paracou	height	%	Satellite	single	0.95	0.96	0.55	0.55
Tapajos	height	%	Satellite	single	0.92	0.91	0.69	0.62
Paracou	BA understory	m^2 ha^{-1}	Inventory	single	0.94	0.90	0.12	0.08
Paracou	Abundance understory	ha^{-1}	Inventory	single	0.99	1.00	342.15	309.81
Paracou	Rank-abundance	ha^{-1}	Inventory	single	0.85	0.93	3.67	3.58
Tapajos	Rank-abundance	ha^{-1}	Inventory	single	0.74	0.94	3.63	3.48
Paracou	GPP	kgC m^{-2} $year^{-1}$	eddy flux	day	0.97	0.60	0.75	0.67
Tapajos	GPP	kgC m^{-2} $year^{-1}$	eddy flux	day	0.97	0.45	1.12	0.67
Paracou	GPP	kgC m^{-2} $year^{-1}$	Satellite	day	0.95	0.45	1.18	0.80
Tapajos	GPP	kgC m^{-2} $year^{-1}$	Satellite	day	0.96	0.22	1.54	0.28
Paracou	LAI	m^2 m^{-2}	Satellite	15 days	1.00	0.69	0.29	0.13
Tapajos	LAI	m^2 m^{-2}	Satellite	15 days	1.00	0.55	0.26	0.17
Paracou	LAI	m^2 m^{-2}	Drone	15 days	1.00	0.84	0.11	0.11
Tapajos	LAI	m^2 m^{-2}	Terrestrial	15 days	1.00	0.25	0.32	0.20
Tapajos	LAI	m^2 m^{-2}	Phenocam	15 days	1.00	0.91	0.11	0.08
Paracou	ET	mm day^{-1}	eddy flux	day	0.96	0.69	0.60	0.60
Tapajos	ET	mm day^{-1}	eddy flux	day	0.96	0.75	0.75	0.63
Paracou	RSWC	%	eddy flux	day	0.97	0.77	0.24	0.13
Tapajos	RSWC	%	eddy flux	day	0.99	0.39	0.20	0.11

1161
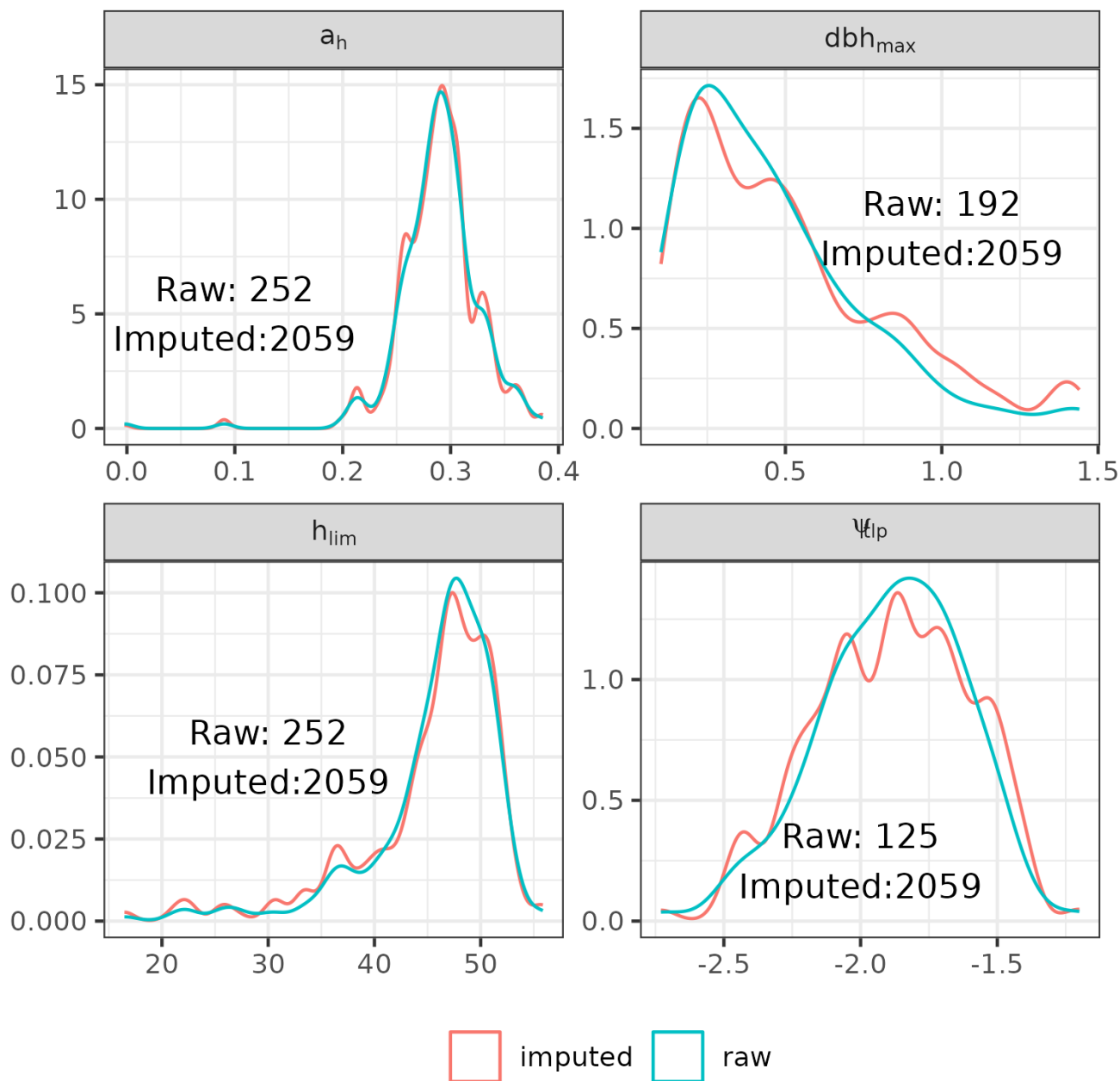
Figure A1: Representativity of imputed functional traits values (red) against raw functional trait values (blue) from various datasets (see methods). Traits were imputed using predictive means matching for dbh$_{max}$, hlim, and π_{tlp} only. The number in each subplots represents the number of species with a trait value in the raw data and after imputation composing respectively the blue and red curves.
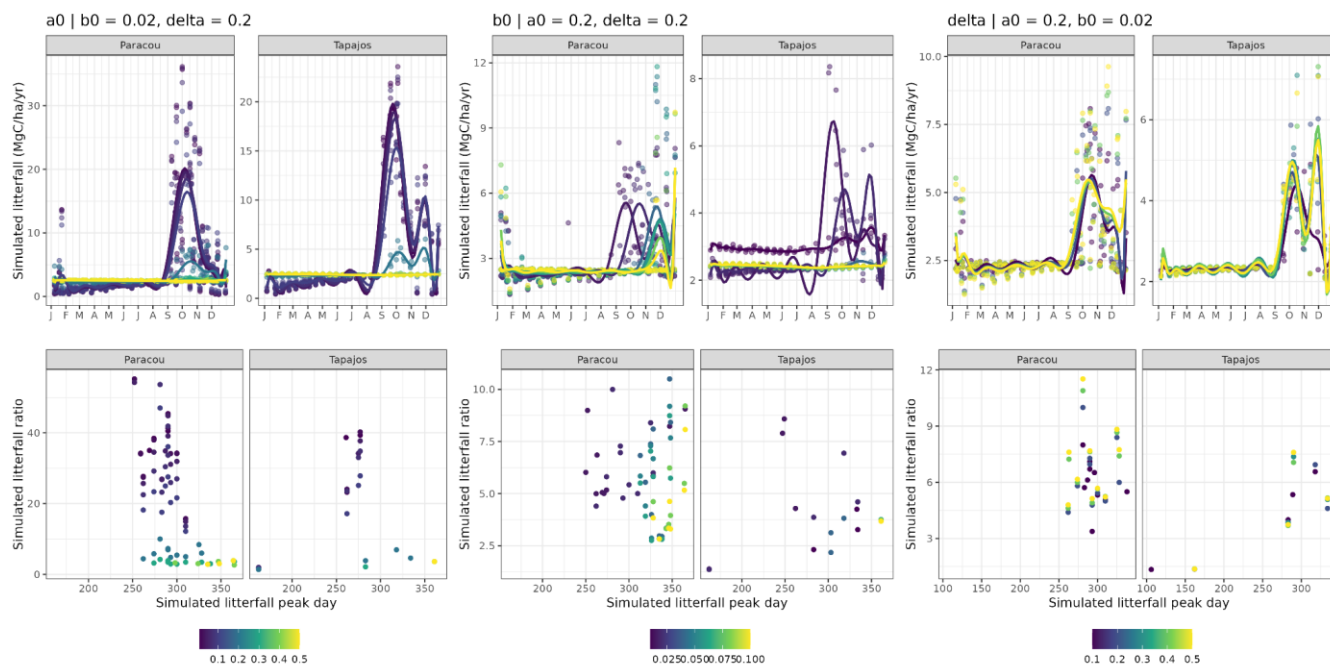
Figure A2. Effect of each parameter of the new leaf shedding module on the simulated timing and intensity of the litterfall peak during the dry season. Top panels illustrate simulated variations of litterfall at both sites for varying $a_{T,0}$, $b_{T,0}$, and δ_0 with the other parameters fixed to a calibrated value. Bottom panels illustrate the corresponding timing and intensity of the dry season litterfall peak: (i) the day of the litterfall peak as the julian day of the maximum annual value (day), and (ii) the ratio between the peak value (computed as the average of litterfall flux over the two consecutive time intervals before and after the peak day) divided by the basal flux (computed as the average between January and April) (ratio). $a_{T,0}$ mainly limited the intensity of the peak with a peak up to 60 times the wet season base litter flux with small parameter values close to 0.01 and no peak with values greater than 0.3, when $b_{T,0}$=0.02 and δ_0 =0.2. Values of $a_{T,0}$ greater than 0.1 also resulted in a later peak during the dry season. $b_{T,0}$ mainly influenced the date of the simulated peak during the dry season, as well as the intensity of the simulated peak for values greater than 0.1. Indeed, low values of $b_{T,0}$, close to 0.01, resulted in a peak starting in September, while high values showed a peak starting in December, when $a_{T,0}$=0.2 and δ_0=0.2. Finally, δ_0 appeared to have a smaller influence on the intensity and timing of the simulated litter peaks. Higher values of δ_0 increased the duration of the simulated peaks or the litter flux between two peaks during the same dry season.
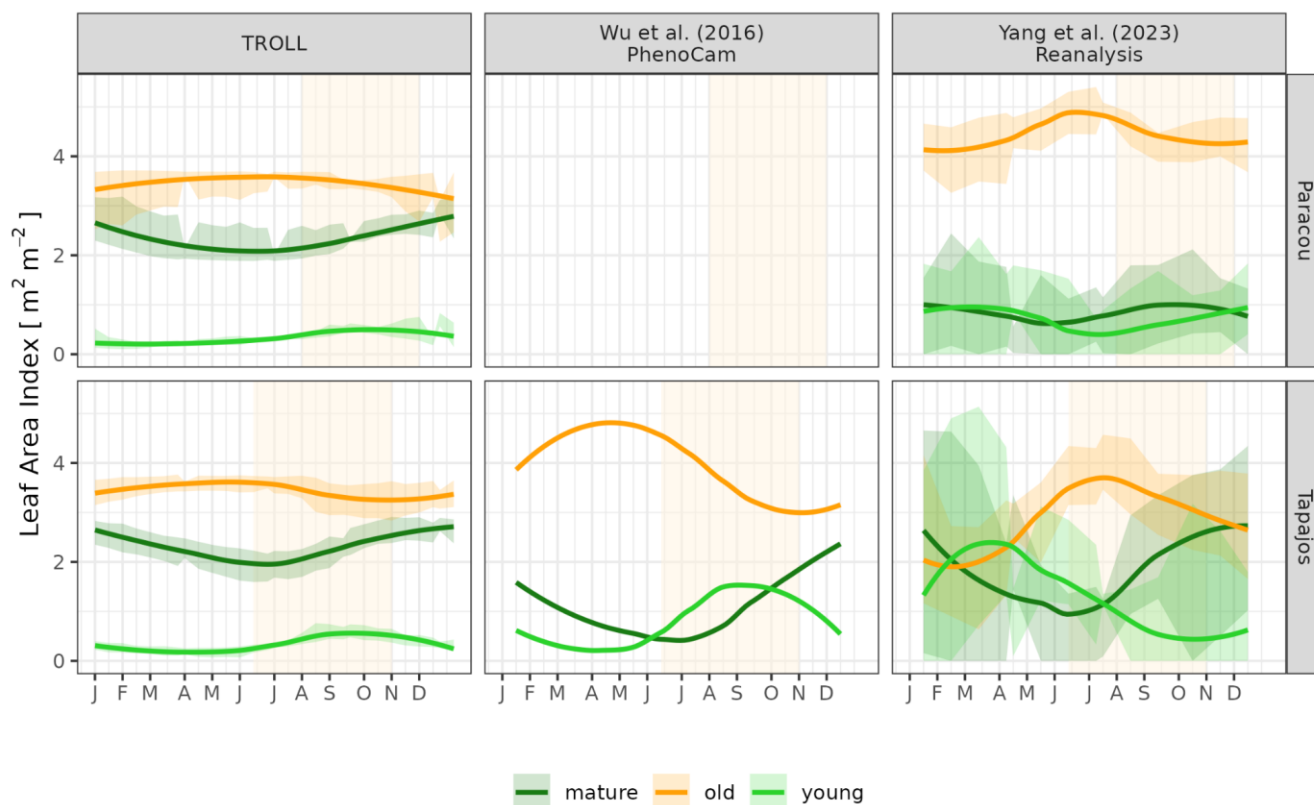
Figure A3: Mean annual cycle of leaf area index per leaf age cohorts, derived from fortnightly means, at Paracou and Tapajos. Note that the three leaf age cohorts (young, mature and old leaves) are not defined the same way in the three sources. Leaf age per cohort depends on the individual leaf lifespan in TROLL 4.0 (see Maréchaux et al., submitted companion paper), while the transition from young to mature and mature to old are respectively fixed to 1.71 and 5.14 months in Yang et al. (2023) and fitted to 1 and 3 months in Wu et al. (2016). Bands are the intervals of means across years, and the vertical yellow bands in the background correspond to the site's climatological dry season.
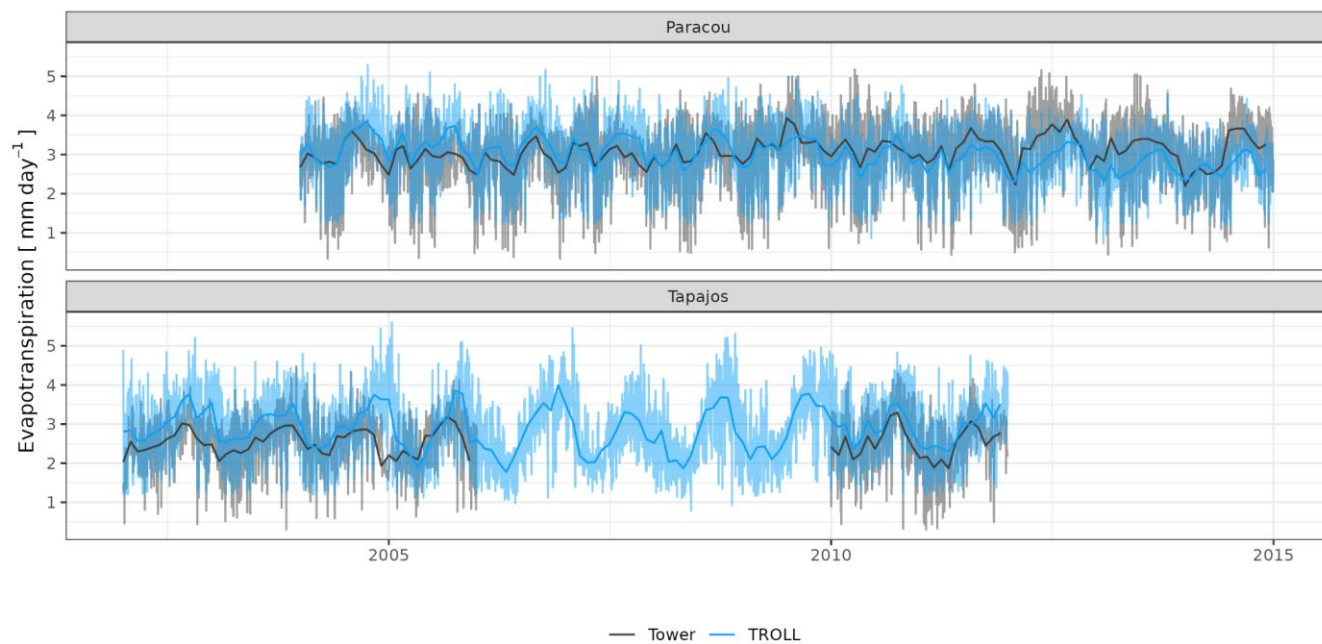
1188

1189
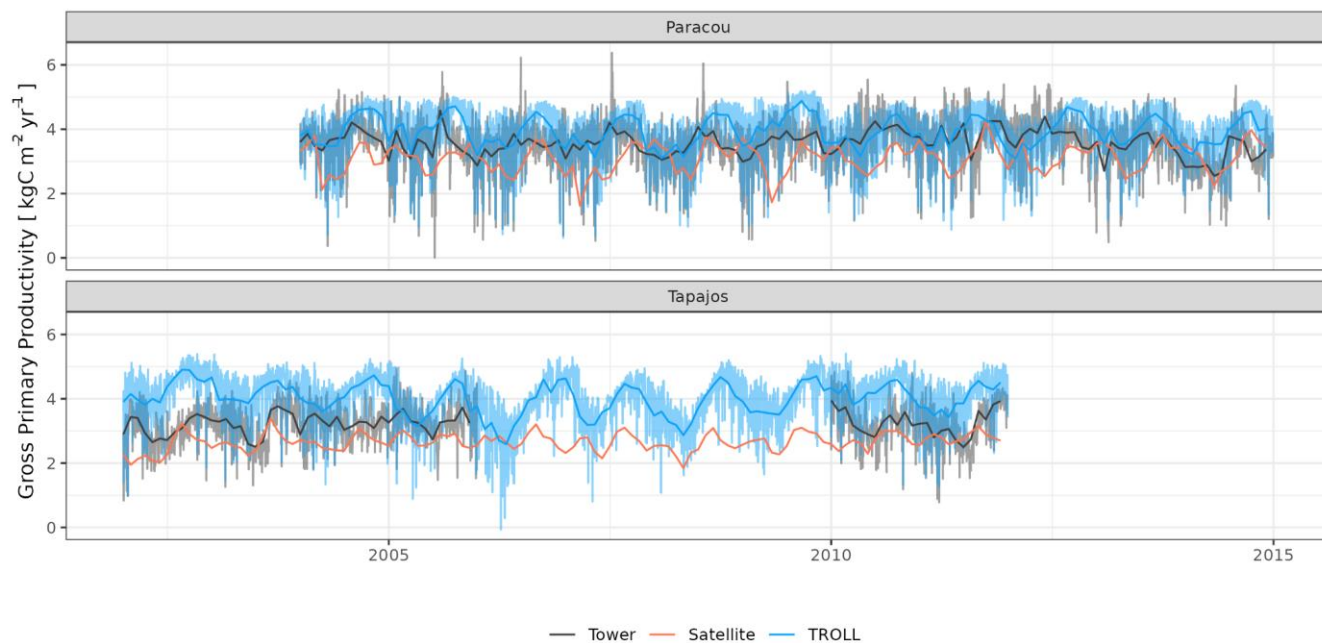
1190

Figure A4: Daily and monthly means of gross primary productivity for Paracou and Tapajos. Dark lines are the monthly means, semi-transparent lines are the daily means variations with the exception of satellite data for which data are available only every 8 days.
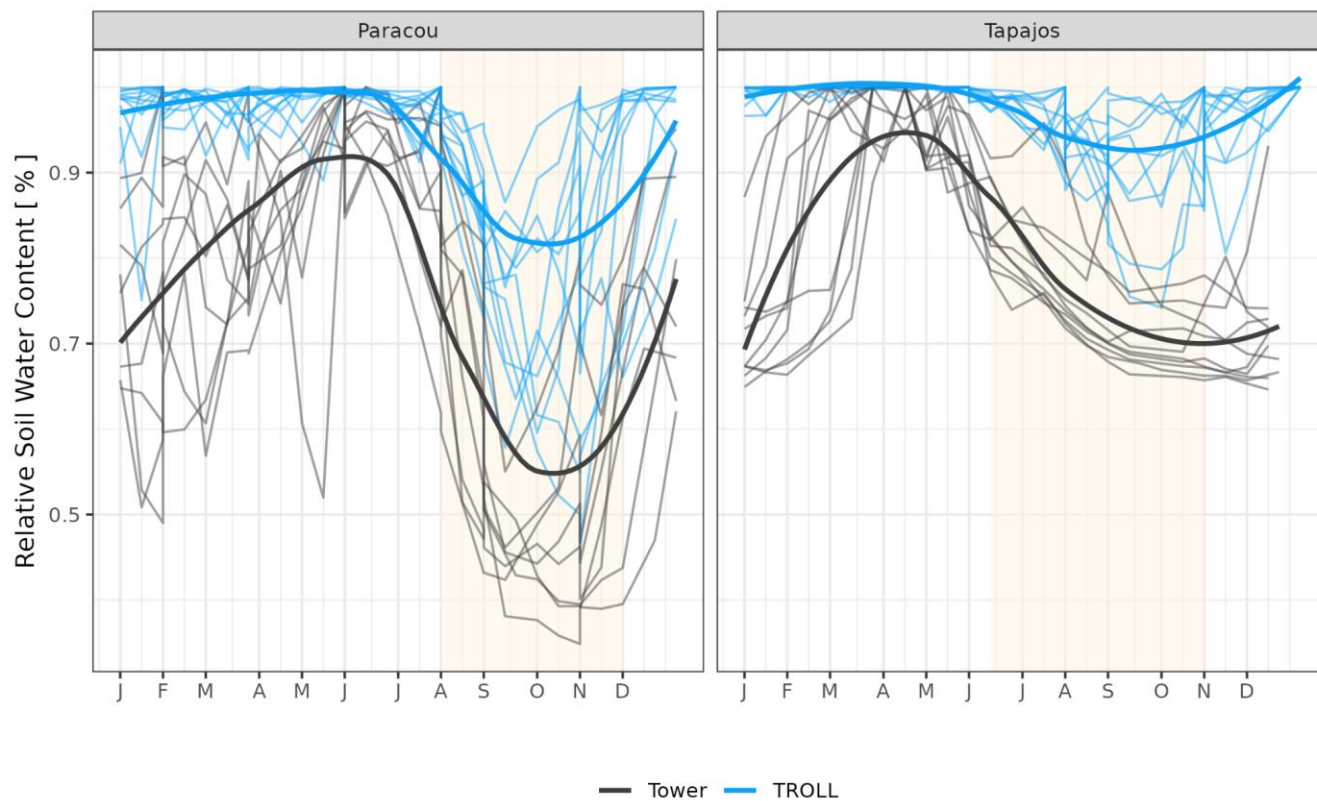
1194

1195

Figure A5: Daily and monthly total of evapotranspiration for Paracou and Tapajos. Dark lines are the monthly means, semitransparent lines are the daily means variations.
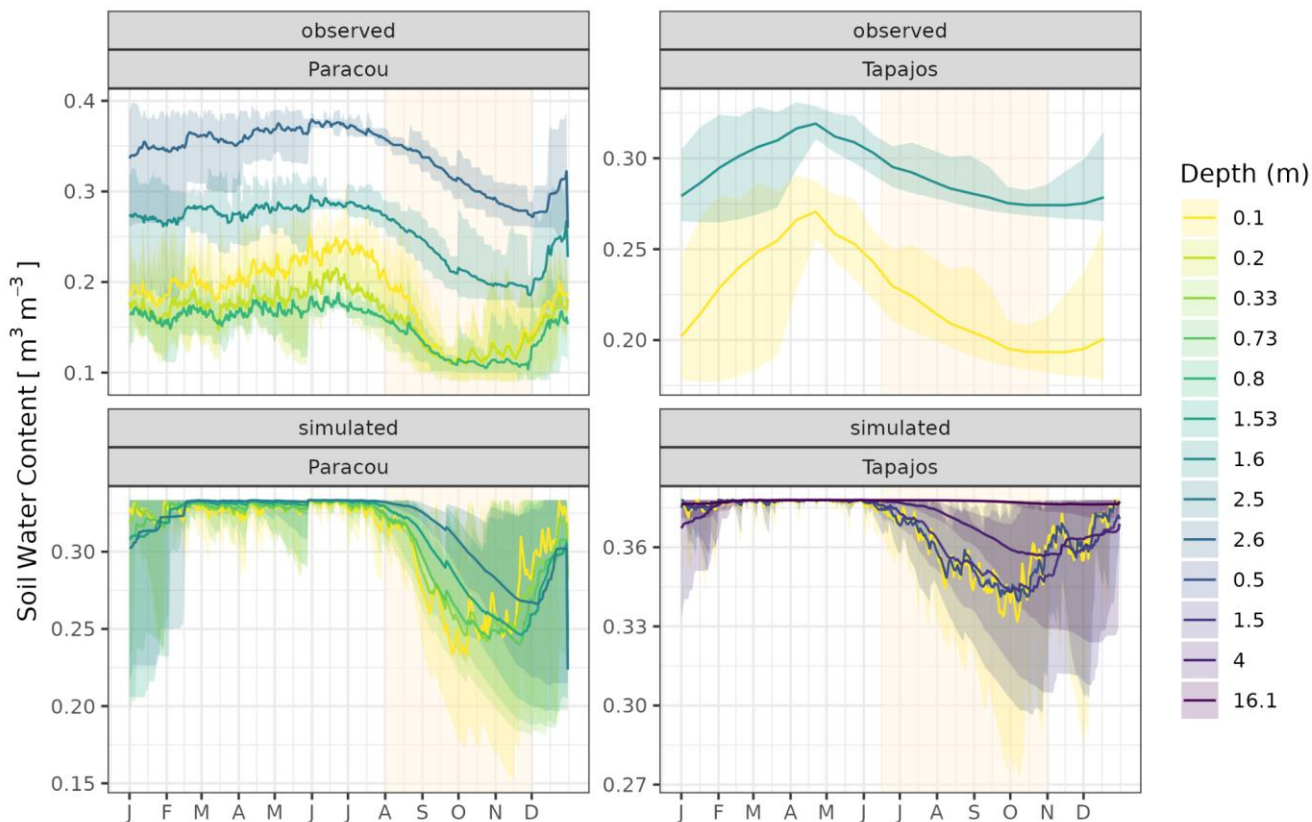
1198

Figure A6: Mean annual cycle from daily means of relative soil water content for Paracou and Tapajos for the topsoil layer up to 10 cm. Dark lines are the daily mean across years, semi-transparent lines are the daily means per year. The vertical yellow bands in the background correspond to the site's climatological dry season.

Figure A7: Mean annual cycle from daily means of soil water content for Paracou and Tapajos at different depths. The depth value indicates the maximum depth of the layer. Dark lines are the daily means across years, and bands are the intervals of means across ten years The vertical yellow bands in the background correspond to the site's climatological dry season.